Article

A novel Adaptive Neuro-Fuzzy based cascaded PIDF-PIDF controller for automatic generation control analysis of Multi-Area multi-source Hydrothermal System

Abinands R [1], Ravi K [1,*] , Jacob I Raglend[1] , Belwin J Edward

[1] School of Electrical Engineering, Vellore Institute of Technology, Vellore, India; abinands.ramshanker2019@vitstudent.ac.in, k.ravi@vit.ac.in; jbelwinedward@vit.ac.in, jacobraglend.i@vit.ac.in

* Correspondence: k.ravi@vit.ac.in;

Abstract: This article investigated the Automatic Generation Control (AGC) of multi-area multi-source interconnected systems with hydropower plants, thermal power plants, and wind energy. In this paper, A technical novelty is present as well as a software novelty of utilizing a novel algorithm. An Adaptive Neuro-fuzzy controller integrated with the cascaded proportional-integral-derivative with filter (PIDF-PIDF) is a new cascaded controller (ANF-PIDF-PIDF) that has been presented as a secondary controller for the applied hybrid power system. In addition to the technical novelty, there exists a software novelty of utilizing the novel Skill Optimization Algorithm (SOA) to optimize PIDF- PIDF controller parameter gains and the Adaptive Neuro-Fuzzy controller's input and output scaling factors. SOA is used to update the controller parameters with integral square error (ISE) employed as the objective function. SOA also outperforms other algorithms in terms of convergence speed and accuracy. The appropriate generating rate constraints (GRC) for the thermal and hydro plants have been considered. A 1% step load disturbance was considered simultaneously in all three areas. The controller's performance is evaluated and compared with and without considering the effects of wind energy sources and non-linearity for ANF-PIDF-PIDF, PIDF-PIDF, and PIDF and it is determined that the ANF-PIDF-PIDF was the most efficient. The dynamic system performance is also compared with parallel high voltage direct current (HVDC) tie-lines. The investigation clearly shows that incorporating HVDC tie-line with multi-area, multi-source provides better dynamic performance in terms of maximum amplitude, oscillation, and settling time. Additionally, sensitivity analysis is done, and the optimum controller gains do not need to be reset to uncertain values in system loading conditions. All simulation results were evaluated using MATLAB 2016b.

Keywords: Automatic generation controls (AGC), Adaptive Neuro-Fuzzy controller, cascaded controller, parallel High voltage direct current (HVDC) tie-lines, Skill Optimization Algorithm (SOA)

1. Introduction

The power system's augmentation and control action are necessitated by its rapid expansion. It is necessary to balance energy production and energy consumption [1]. The Automatic Generation Control (AGC) is critical in ensuring that the frequency variations remain below acceptable bounds. The primary objective of AGC is to maintain the frequency deviation within acceptable limits and also control the power transfer between different locations. It is critical for managing the power variations along the tie lines. An interconnected power system with several producing sources, such as hydropower plants, thermal power plants, and renewable energy sources, among others, could have several generating sources in its control areas. A more complicated control structure is required when several sources of renewable energy are injected into power

 doi:10.20944/preprints202211.0422.v1

systems. In multi-source interconnected power systems, frequency variation is, in essence, the leading cause of variation. While maintaining suitable production, distribution, and customer load requirements, AGC's main objectives are to preserve frequencies and tie-line power variations within specific limits. In an integrated power system, the governor regulation and load frequency control cooperate to keep the system frequency deviation low [2]. The primary goal of lowering the area control error (ACE) is to maintain the frequencies and tie-line power within specified bounds [3]. Soft computing techniques and Artificial intelligence is now widely used in a variety of fields. The optimum fuzzy control strategy governs the power flow in this power system problem. Electric power systems must now be operated in real-time by intelligent systems that draw knowledge, skills, and procedures from different sources due to the expanding scale and complexity of the sector as well as the increase in power consumption.

Many papers look at different areas of AGC design, such as illustrating the effectiveness of power systems' dynamic performance. The earliest test to adjust the power system's frequency used a flywheel and the power unit's speed governor. However, this method was insufficient for the power systems to function correctly. As a result, the power unit's speed governor added a supplementary control method based on the frequency deviation (Δf) signal and its integral. Tasnin et al. in [4] has defined the traditional AGC techniques in power systems. The most popular non-conventional energy source used to provide consumer electrical energy is wind power plants [5]. Hakimuddin et al. in [6] investigated the efficacy of AGC in thermal, hydro, and wind power plants. While changes in the amount of wind energy available to wind turbines can cause an increase or decrease in the imbalance between generation and load demands, combining WPPs with traditional power plants causes system instability. AGC is also used in conventional power plants, but because wind energy is stochastic, WPPs may cause disturbances [7]. Currently, wind power plants are not used to control and stabilize perturbations in the control region. They may, however, have the potential to participate in the design of AGC power systems. Furthermore, wind power plant dynamics are not included in the power system control regions model [8]. AGC is used to correct the disturbed problems and restore the frequency of the system. The work done in [9] shows two components of integrated hydro-thermal systems with a wind farm. The work done in [10] evaluated system dynamic frequency responses for three-area thermal systems, one of which incorporated a solar thermal power plant (STPP). Three diverse area thermal systems namely, hydro, wind, and solar photovoltaic plants were evaluated in the work done in [11]. Some authors examined the frequency response of various techniques in AGC investigations. The load-generation imbalance of a practical power system affects tie-line power flow and the system's nominal frequency [12]. The authors documented the effects of renewable energy sources such as solar photovoltaic panels, wind and frequency regulation on automatic load frequency control (ALFC) studies in the work done in [13]. The authors investigated the synchronous generator excitation issue of two-area reheating thermal systems, such as PV arrays and wind, while taking into account system non-linearity like GRC. The work done in [14] reports some control algorithms for designing the additional ALFC loop controller. Traditional controllers, however, might not even react adequately when the operational state of the power system changes if they are programmed for a specific ALFC working state. With a typical controller set to a single functional form, it isn't easy to establish stability across the system's whole working range due to its nonlinearity. To solve this problem and efficiently run the power generating units, frequency, and tie-line power flow, intelligent control technology such as the FLC is advised over the traditional one [15]. The Fuzzy logic controller increases the traditional controller's closed-loop effectiveness and can manage every variation in operational points by modifying controller parameters live. The researchers' primary focus in the combined AGC experiments has been designing the ALFC loop controller. The auxiliary controller of the ALFC loop, like traditional PID, fuzzy-PID, and Neuro-fuzzy-PID, with HVDC, has been done in the integrated LFC and automatic voltage regulator (AVR) inner loops in the work done in [15,16]. Abazari et al.

 doi:10.20944/preprints202211.0422.v1

[17] demonstrated load frequency control Power Systems using a classical PID & Fuzzy PID controller. They proposed modeling a PID and fuzzy PID-based LFC controller to reduce the power system's frequency deviation. Furthermore, compared to traditional PID controllers, it achieves an entire system with a shorter settling time, minimizes the peak amplitude of the characteristic frequency variations, and minimizes the power of the exchanged tie line. However, more fine-tuning and simulation are required before it can be used; issues with locating appropriate membership values for fuzzy systems. Prakash et al. [18] employed one of the artificial intelligence approaches to investigate the LFC of interconnected system frameworks. They suggested modeling a PID and an artificial neural network (ANN) PID-based load frequency control to minimize the power system's frequency deviation. As a result, the intelligent control strategy based on ANNs is faster and more accurate, yielding better results. However, large amounts of data are required for training; neural networks can only be used if training data is available, and the learning process can be time-consuming. As a result, load frequency control research can be investigated by combining the advantages of neural networks and fuzzy logic controllers with traditional controllers. There has yet to be any prior research on the optimal Neuro-fuzzy controller integration with adaptive Neuro-Fuzzy cascaded PIDF-PIDF controller.

Moreover, in the previous research on load frequency control, seven membership functions with 7*7=49 rules were considered for the fuzzy controller design. However, more resolution is required to optimize the heavily loaded power system. As a result, the authors altered the eleven-membership function, resulting in 11*11=121 Rules for dealing with the complex dynamic framework. The gain parameters must be carefully chosen when developing an efficient controller for the area control system; the gain parameters must be carefully chosen. Different studies have proposed and validated different soft computing strategies for obtaining control parameters for system performance optimization. Because of this, making an accurate selection of the controller gain is quite important for achieving better regulated performance. In recent years, by the year 2015, many bio-inspired algorithms have been developed to optimise the controller gain values. These algorithms include: 1) direct synthesis (DS) for tuning of PID controller parameters [21], 2) grey wolf optimizer algorithm for tuning of PI and PID controller gain values [22], 3) self adaptive modified bat algorithm (SMBA) for tuning of PI controller [23], 4) Cuckoo search (CS) algorithm for tuning of PI controller [24], 5) teaching learning based optimization [25] 6) hybrid particle swarm optimization (PSO) and pattern search (PS) (hPSO-PS) optimization for tuning of fuzzy PI controller [26], 7) a minority charge carrier inspired (MCI) method was suggested for tuning the I and PI controller [27], and 8) a modified harmony search algorithm (MHSA) was suggested for adjusting the parameters of the PID controller [28]. More recently, the Genetic Algorithm(GA)[29], Tabu Search(TS)[30], Simulated Annealing(SA)[31], Differential Evolutionary Algorithm(DEA)[32], Particle Swarm Algorithm(PSO)[33], Immune Algorithm(IA)[34] were all also utilized for tuning PID controllers. Table 1 presents the advantages and disadvantages of various metaheuristic algorithms.

Preprints (www.preprints.org) | NOT PEER-REVIEWED | Posted: 22 November 2022 doi:10.20944/preprints202211.0422.v1

Table 1 : Advantages and Disadvantages of different algorithms

ALGORITHM	MAJOR ADVANTAGE	MAJOR DISADVANTAGE
GA [29]	Simple to understand and put into practice Does not require prior understanding of maths	There is no guarantee of a solution that is optimal we are unable to solve a wide variety of different kinds of complicated optimization issues. The propensity to converge in the optimal solution for the immediate environment
TS[30]	Escapes from local minima as well by using the "tabu list"	A sluggish pace of convergence The ineffective approach to solving the high-dimensional problem
SA[31]	Can give a solution even in a huge search area. Easy to understand and apply Provides pretty excellent solutions for certain optimization issues	A sluggish pace of convergence a lack of capacity to find solutions to difficult multifaceted issues Performance decline in big dimension issues
DEA[32]	Possesses the ability to solve multidimensional, non-differential, and non-continuous problems;	Difficult to choose the appropriate control settings There is no guarantee of the accuracy of the solution.
PSO[33]	It Converges rapidly; It is capable of resolving complicated optimization issues in a variety of application areas.	The unfavourable impact on the solutions brought about by the incorrect selection of control factors The risk of becoming mired at a particular region's minimum point Poor performance in high-dimensional as well as multimodal optimization
IA[34]	It is adept at the search exploration process.	Poor utilisation of the search
SOA	High Convergence rate Can solve complex multidimensional problems It is faster and requires less iterations	It is a little complex to understand

We utilize a novel algorithm for the very first time in this application named the Skill Optimization Algorithm. SOA has been tested on multiple functions and has been determined to be better than all the above mentioned algorithms in terms of convergence speed. The SOA based ANF-PIDF-PIDF controller is compared with GA and PSO to show that it is much more efficient than the conventional algorithms. There has been no research till now conducted by using SOA-based AGC to improve the gains of standard PIDF-PIDF and the input-output scaling factors of Neuro-Fuzzy controllers.

 doi:10.20944/preprints202211.0422.v1

The cascade controller improves the dynamics system over a single controller since it has many configurable parameters. Furthermore, the cascade control technique is renowned in the control system for its quick disturbance rejection before transmission to other system components. The earlier literature review presents a new hybrid control structure for the unified ALFC-AVR system, including Fuzzy logic control and the cascades controller PI and PIDF. Frequency variation and ACE are the two input signals that the controller receives. According to the literature, the ALFC loop and the choice of controller settings improve the system performance of the researched system in the combined adaptive Neuro-Fuzzy cascaded PIDF model. Traditional methods may not deliver the best results for a plan with nonlinear constraints. Different studies have proposed and validated different soft computing strategies for obtaining control parameters for system performance optimization [20].

The proposed controller must handle small variations in the system's state without affecting stability. [16] Performed a sensitivity study by altering the amount and position of the step load disturbance (SLD). The resilience of the 50% loading circumstances, skill optimization algorithm, enhanced adaptive Neuro-Fuzzy-cascaded PIDF inputs gains, and Neuro-Fuzzy inputs-output scaling factors and other parameters must be evaluated against a wide range of systems loading conditions.

Because it has more configurable parameters than a single controller, the cascade controller improves the dynamics system over a single controller. Furthermore, the cascade control technique is renowned in the control system for its quick disturbance rejection before transmission to other system components. The research done also explores a new hybrid control structure for the unified ALFC-AVR system, which includes fuzzy logic control and the cascades controllers PI and PIDF. Frequency variation and ACE are the two input signals that the controller receives. According to the literature, the ALFC loop and the choice of controller settings improve the system performance of the researched system in the combined adaptive Neuro-Fuzzy cascaded PIDF model. Traditional methods may not deliver the best results for a plan with nonlinear constraints

In addition to the maiden application of the novel optimization algorithm, we have also incorporated technical novelties with regard to power system stability with the help of AGC. Many researchers stated that the AGC considers ALFC and AVR loops, focusing on traditional and non-traditional controllers, as demonstrated in the literature review. Little attention was paid to several aspects such as, including source type, controllers, optimization techniques, sensitivity analysis using altered generator characteristics, variation in the water inertia time constant (T_w), the synchronization correlation coefficient of AC tie lines with system loading conditions, and the effects of a parallel HVDC tie line for stability analysis. This article investigates the optimal design and implementation of the cascaded adaptive Neuro-Fuzzy-PIDF-PIDF-based AGC controller for a three unequal area multi-sources power system network comprising hydro and thermal power plants and wind power plants (WPPs). The dynamic response of the optimum AGC controller is measured and compared to that of a PIDF controller. SOA adjusted conventional AGC controller that has also been built in the research in the presence of a 1% step load perturbation in one of the control areas. Additionally, the effect of wind energy sources on the AGC scheme has been investigated when the amount of wind energy to the wind power plants (WPPs) reduces/increases load perturbations in one of the control areas.

1.1. System Design Challenges

The active power balance in the power system is required for frequency stability. When a disturbance occurs in the system, such as a short-circuit fault, trip, tie-line breaking, system disintegration, etc., the total generation and load power may become imbalanced.

 doi:10.20944/preprints202211.0422.v1

The biggest challenges to fixing this issue are as follows:

1. Using a novel AGC controller, we should effectively reduce changes in system frequency, deviation, and tie-line flows from their specified areas. The developed controller should produce system responses with the least settling time, undershoots, and overshoots possible.
2. Finding and implementing the perfect optimization strategy for adjusting the developed controller's parameters.
3. Finding the perfect performance indices for adjusting the developed controller's parameters
4. When applied to various power system models, the new modeling technique must deliver superior results in comparison to conventional systems
5. The design method must be robust.

This article investigates the optimal design and implementation of the SOA optimized cascaded adaptive Neuro-Fuzzy-PIDF-PIDF-based AGC controller for a three unequal area multi-sources power system network comprising hydro and thermal power plants and wind power plants (WPPs). The cascade controller improves the dynamics system over a single controller since it has many configurable parameters. Furthermore, the cascade control technique is renowned in the control system for its quick disturbance rejection before transmission to other system components.

1.2. The primary objectives and achievements

The following objectives have still to be examined based on the extensive literature review.

- To develop three multi-source, unequal-area hydro-thermal systems integrated with wind turbines in the presence of linearity and non-linearity.
- For the input and output scaling factors, as well as the system's built-in PIDF gains. The skill optimization algorithm (SOA) is used to optimize adaptive Neuro-fuzzy controllers, and the present controllers are acquired by assessing dynamic performances of the system.
- To establish which is best, the dynamic performance of the proposed adaptive Neuro-fuzzy-PIDF-PIDF (NF-PIDF-PIDF) controller is compared to that of the classical PIDF-PIDF and PIDF controller.
- To evaluate the sensitivity analysis by altering the characteristics of the generators while accounting for a system loading ± 25%.
- To investigate the effects of non-linearity requirements on the system using the present adaptive NF-PIDF-PIDF controller.
- To investigate the effects of parallel HVDC tie-line on the system using the present adaptive NF-PIDF-PIDF controller.
- To demonstrate how the water inertia time constant (T_w) varies in loading systems, to evaluate the sensitivity analysis by altering the generators' parameters, and to verify the sensitivity of the present NF-PIDF-PIDF controller.
- To show how the suggested controller outperforms the SOA optimum PIDF-PIDF and PIDF controllers created for the AGC power system presented in (i).

The primary contribution of this paper is the design of a novel optimal integration Neuro-Fuzzy-PIDF-PIDF (NF-PIDF-PIDF) controller for different power system models that perform more dynamically than other previously published papers.

The rest of this paper is summarized as the following organization:

Section-2 presents a detailed system design with mathematical equations, system investigation, modeling of the proposed ANF-PIDF-PIDF controller and optimization tech-

Preprints (www.preprints.org) | NOT PEER-REVIEWED | Posted: 22 November 2022 doi:10.20944/preprints202211.0422.v1

nique, Section-3 reveals the simulation and discussion of the detailed results. The article is concluded in Section-4, followed by a list of references and an appendix.

2. Materials and Methods

2.1. Frequency Response Modeling

2.1.1. Reheated thermal power turbine modeling

Each area uses a conventional power system generating plant, as depicted in Figure.2. Reheated Thermal Power (RTP) is implemented using a speed governor mechanism and a turbine with a re-heater, as shown in a thorough block diagram.

The following are the transfer function models for the reheated turbine (GTRT) and speed governing method (GGRT) [11].

$$\text{GGRT(s)} = \frac{1}{1+sT_{grt}} \text{ and GTRT(s)} = \left(\frac{1}{1+sT_{trt}}\right)\left(\frac{1+sK_rT_r}{1+sT_r}\right) \quad (1)$$

Where $T_{grt}$and T_{trt} are the governor and turbine time constants, respectively, and K_r and T_r are the reheated thermal power plant's re-heater gain and time constant, respectively.

2.1.2. Hydro Power Turbine Modeling

A turbine unit in power systems transforms natural energy, like water energy, into mechanical power (P_m), which is then delivered to the generator. The authors commonly utilize a simplified inelastic penstock model without the water hammer effect in power system analysis. The following transfer function(T.F.) is obtained using a simple prime mover model with a single water time constant T_w [14].

$$T.F. = \frac{\triangle P_m(s)}{\triangle P_v(s)} = \frac{1 - T_wS}{1 + 0.5T_wS} \quad (2)$$

The water starting time is T_w in this case, the time it takes for a head H_o to accelerate the water in the penstock from rest to velocity V_o. It is worth noting that Tw varies depending on the load $\frac{l_p v_{po}}{g h_{go}}$ is the answer. T_w at full load is usually varied between 0.5 and 4.0 seconds. Equation (2) depicts a hydraulic turbine's traditional transfer function. For an ideal lossless turbine, it depicts how the turbine power output varies in reaction to changes in gate opening. A simple hydro turbine's block diagram is depicted in Figure 1.

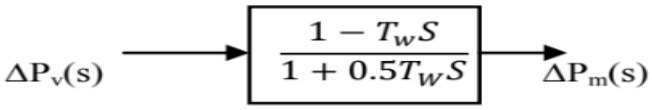

Figure1. Turbine Block Diagram

Equation (3) states that the hydro turbine head alters the water acceleration in the penstock.

$$(\rho l_p A_p)\frac{d\Delta v_p}{dt} = A_p(\rho g)\Delta h_g \quad (3)$$

Where

- l_p is the penstock length.
- v_p is water velocity in the penstock.
- A_p is the pip cross-sectional area.
- ρ is the mass density of water.
- g is the gravity acceleration.
- $(\rho l_p A_p)$ is the mass of water in the penstock.
- $(\rho g)\Delta h_g)$ denotes the incremental pressure varies atthe hydro turbine gate.

Preprints (www.preprints.org) | NOT PEER-REVIEWED | Posted: 22 November 2022 doi:10.20944/preprints202211.0422.v1

Using equation (3) make normalized by dividing both sides by $A_p g h_{go} v_{po}$, to normalize the Equation (3), and obtain (4)

$$\frac{l_p v_{po}}{g h_{go}} \frac{d}{dt}\left(\frac{\Delta v_p}{v_{po}}\right) = -\frac{\Delta h_g}{h_{go}} \tag{4}$$

(5)

$$T_w = \frac{l_p v_{po}}{g h_{go}}$$

The mass flow rate in the penstock is calculated as $q_o = A_p v_{po}$, where q_o is the product of pipe area and water velocity in the penstock. Inserting v_{po} into the equation (5) yields the water's starting time is given by (6).

$$T_w = \frac{l_p q_o}{g A_p h_{go}} \tag{6}$$

Equation (6) calculated the hydro turbine time constant or T_w under variable plant loading (PL). I. Pan et al. in [35] describes the penstock's hydro turbine gate valve opening (V_o) versus water flow rate. The mathematical description of water flow rate in terms of V_o is given in (7).

$$q(p.u) = \frac{1}{10^4}(\%V_o)^2 \tag{7}$$

A change in the plant loading has caused the V_o to change. Therefore, equation (7) can be expressed in plant loading, as illustrated in (8).

$$q(p.u) = \frac{1}{10^4}(\%P_L)^2 \tag{8}$$

Using equation (6) and equation (8)

$$T_w = m \times 10^{-4} \times (\%P_L)^2 \tag{9}$$

Where $m = \frac{l_p q_o}{g A_p h_{go}} = 4$

As a result, equation (9) demonstrates that T_w varies with the P_L load levels.

2.1.3. Wind Power Plant Modeling

The wind's kinetic energy is transformed into mechanical energy by rotating machines known as wind turbines. After that, the electrical grid receives this mechanical energy and turns it into electricity. The generator and rotor of turbines accomplish these energy transformations. The rotor is the main part of the turbine which contains the hub and blades. The turbine's hub rotates as wind strikes the blades due to aerodynamic forces. This rotation is then sent to the transmission mechanism, which reduces the rotations per minute. The transmission system is composed of the important bearing, high-speed shaft, gearbox, and low-speed shaft [36]. The pitch angle control system ensures that the desired pitch angle is maintained regardless of wind speed, allowing wind turbine production to be adjusted regardless of wind speed. The hydraulic pitch actuator data fit pitch response, and blade characteristics are included in the mathematical analysis of the wind power plant. Modeling the wind farm system, pitch control, hydraulic pitch actuator, data fit pitch response, and induction generator are all described in detail below [37].

$$G_P(S) = \frac{K_{WP1}(1+ST_{WP1})}{(1+S)} \tag{10}$$

Preprints (www.preprints.org) | NOT PEER-REVIEWED | Posted: 22 November 2022 doi:10.20944/preprints202211.0422.v1

$$G_H(S) = \frac{K_{WP2}}{(1+ST_{wp2})} \quad (11)$$

$$G_D(S) = \frac{K_{WP3}}{(1+ST_{wp3})} \quad (12)$$

$$G_1(S) = \frac{1}{(1+ST_w)} \quad (13)$$

The output of wind power deviation can be written as:

$$\Delta P_{P_m} = K_{fc} G_1(S) \quad (14)$$

Where K_{wp1} and T_{wp1} are the pitch control systems gain and time constants, K_{wp2} and T_{wp2} are the gains for hydraulic pitch actuator gain and time constant, K_{wp3}, T_{wp3} data appropriate pitch response gain and time constant, and K_{fc} is fluid coupling.

2.1.3.1. The Effect of Wind Power Integration on Grid Frequency Stability

The active power balance is a prerequisite for the power system's frequency stability. The total generation power and the total load power may be out of balance when a disturbance in the system (such as a short-circuit fault, trip, tie-line breaking, system disintegration, etc.) occurs. The system frequency will increase if the total generation power exceeds the total load power (including grid losses). In contrast, it will decrease if the total generation power is less than the total load power. The associated steps, mainly regulating the active generator output, disintegrating the generator, disintegrating the load, and so forth, shall be adopted based on the various frequency variations and the real operation condition of the system. Frequent regulation is essential for the electrical system to run securely and reliably [38]. In order to maintain frequency security and frequency stability during continuous operation of the power system once wind power is incorporated into the grid, it has become one of the main topics in wind power research as wind power penetration rises. The system inertia will be critical in determining the rate of variation of the system frequency in the event of a fault when the grid frequency is drastically lowered. The lower the inertia, the quicker the system frequency drops. Any decrease in inertia response puts the power system at risk for a significant frequency accident.

The security of a power system is defined as its capacity to endure disruptions without experiencing a breakdown. Wind turbines must be able to ramp up and down in order to prevent insecure power system operation. Wind turbines must be able to avoid excessive fault levels while also assisting with fault identification and also must be able to contribute to both voltage and frequency control to stabilize the power system following a disturbance [39].

2.1.4 Governor and Generator Modeling

2.1.4.1 Governor Modeling

In reaction to changes in load, the turbine controlling system's primary goal is to control turbine speed, which affects the frequency and active power. In power systems, governors are employed to detect the frequency bias brought on by a change in load and negate it by adjusting inputs to turbines. The speed governing mechanism can be classified into two categories namely, Electric Governor and Mechanical Governor[40]. The transfer of electrical governor is given as -

$$G_{tEg} = \frac{k_{dh}s^2+k_{ph}s+k_{ih}}{k_{dh}s^2+\left(k_{ph}+\frac{f}{R}\right)s+k_{ih}} \quad (15)$$

Preprints (www.preprints.org) | NOT PEER-REVIEWED | Posted: 22 November 2022 doi:10.20944/preprints202211.0422.v1

Where K_{dh}, K_{ph}, *and* K_{ih} electric governor derivative, proportional, and integral gains, respectively

The transfer function of the Mechanical Governor is given as -

$$U_{kg} = \frac{Kg}{Tgs+1} \tag{16}$$

where k_g and T_g mechanical governor constant gain and governor time constant respectively

2.1.4.2 Generator Modeling

A generator power system converts mechanical energy from a turbine to electrical energy. The mechanical power conveyed by the turbine is no longer equal to the electrical power produced by the generator when the load changes. The error is between mechanical (P_m) and electrical power (P_e) is incorporated into the rotor speed variation r, which could be multiplied by 2π to get the frequency bias Δf [41].

$$\frac{2H}{Ws}\frac{d\Delta w}{dt} = \Delta P_m - \Delta P_e \tag{17}$$

In terms of a slight speed difference

$$d(\frac{\Delta W}{Ws})dt = \frac{1}{2H}(\Delta P_m - \Delta P_e) \tag{18}$$

Speed is measured in units per second.

$$\frac{d\Delta W}{dt} = \frac{1}{2H}(\Delta P_m - \Delta Pe) \tag{19}$$

The LFC closed Loop

$$\Delta P_T - \Delta P_D = \frac{2W}{f^0}\frac{d}{dt}(\Delta f) + D\Delta fMW \tag{20}$$

The preceding equation, after Laplace transformation, produces

$$\begin{aligned}\Delta P_T(s) - \Delta P_D(s) = \frac{2W}{f^0} s \frac{d}{dt}\,\Delta f(s) + D\Delta f(s)MW \\ = \left[\frac{2w}{f^0}s + D\right]\Delta f(s) \;\; \text{i.e} \\ \Delta f(s) = \frac{1}{\frac{2H}{f^0}}[\Delta P_T(s) - \Delta P_D(s)]\end{aligned} \tag{21}$$

$$\Delta f(s) = G_p(s)[\;\; \Delta P_T(s) - \Delta P_D(s)] \tag{22}$$

where

$$G_p(s) = \frac{1}{\frac{2H}{f^0}+D} = \frac{1/D}{(1+\frac{2H}{f^0 D})} = \frac{K_P}{1+STP} \tag{22.1}$$

$$K_P = \frac{1}{D}T_P = \frac{2H}{f^0 D}, \tag{22.2}$$

$$f = f^0 + \Delta f \tag{22.3}$$

$$D = \frac{P_{Lp.u}}{f^0} \tag{22.4}$$

Preprints (www.preprints.org) | NOT PEER-REVIEWED | Posted: 22 November 2022 doi:10.20944/preprints202211.0422.v1

Where P_m is mechanical input power in per-unit, P_e is electrical output power in per-unit, H is the inertia constant, ΔW is the synchronous rotor speed, D load damping constant and f is nominal frequency, f^o is operating frequency, Δf frequency deviation.

2.1.5 AGC of three-area interconnected power system

Multi-control regions are present in any interconnected power network all generators in power systems are believed to work together an analogous turbine generator and governor system can be installed in the proposed research investigated three areas interconnected in a ring topology as illustrated in Figure.2.

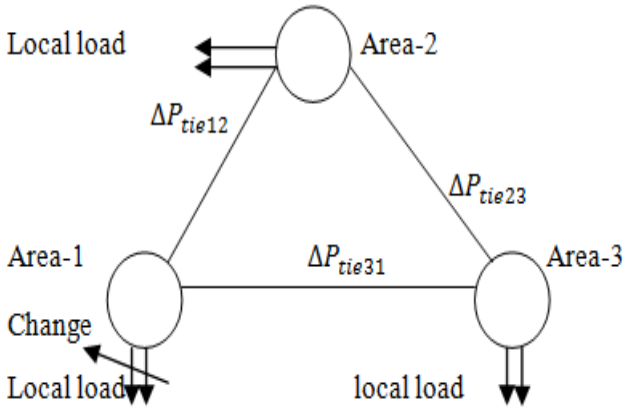

Figure.2. Three area models were linked by ring topology.

The real power delivered through the tie-line is indicated is given equation (23) during the regular operation of the power system.

$$P_{12} = \frac{V_1 V_2}{X_{12}} \sin(\delta_1 - \delta_2) \tag{23}$$

Where δ_1 and δ_2 are the respective power angles of machines that are identical and X_{12} is the tie-line reactance. At the comparable machines in areas 1 and 2, the voltages are V_1 and V_2, respectively.

To obtain the tie power deviation as shown in equation (23), the authors reformed equation (24) for a small tie-line flow P_{12} around an equilibrium point δ_{01} δ_{02}.

$$\Delta P_{12} = P_{S12} (\Delta\delta_1 - \Delta\delta_2) \tag{24}$$

The synchronizing power coefficient P_s can be calculated using equation (25).

$$Ps = \frac{dp_{12}}{d\delta_{12}}|_{\delta_{12}^\circ} = \frac{E_1 E_2}{X_{12}} \cos(\delta_1^\circ - \delta_2^\circ) \tag{25}$$

When the relationship between speed and area power angle speed is considered, equation (25) could be expressed as equation (26).

$$\Delta P_{12} = Ps_{12} (\int \Delta\omega_1 - \int \Delta\omega_2) \tag{26}$$

where $\Delta\omega_1$ and $\Delta\omega_2$ are the speed variations in areas 1 and 2, respectively. The equation (27) is obtained by taken the Laplace transformation function of equation (26).

Preprints (www.preprints.org) | NOT PEER-REVIEWED | Posted: 22 November 2022 doi:10.20944/preprints202211.0422.v1

$$\Delta P_{12}(s) = Ps_{12}S\,(\int \Delta\omega_1(s) - \int \Delta\omega_2(s)) \tag{27}$$

Similarly, the difference in tie-line power between areas 1 and 3 is given Eq. (28).

$$\Delta P_{13}(s) = Ps_{13}S\,(\int \Delta\omega_1(s) - \int \Delta\omega_3(s)) \tag{28}$$

Equation (27) and equation (28) is used the overall change in tie-line power transfer between area-1 and the other two areas in equation (29).

$$\frac{1}{s}\left[\sum_{j=2,3} Ps_1\Delta\omega_1 - \sum_{j=2,3} Ps_{1j}\Delta\omega j\right] \tag{29}$$

The load causes the variation in the tie-line transfer power for those areas in the provided location; the tie-line power deviation (ΔP_{tie}) could be added to the mechanical power variation (ΔP_m) and area load perturbation P_L using a relevant sign.

Preprints (www.preprints.org) | NOT PEER-REVIEWED | Posted: 22 November 2022 doi:10.20944/preprints202211.0422.v1

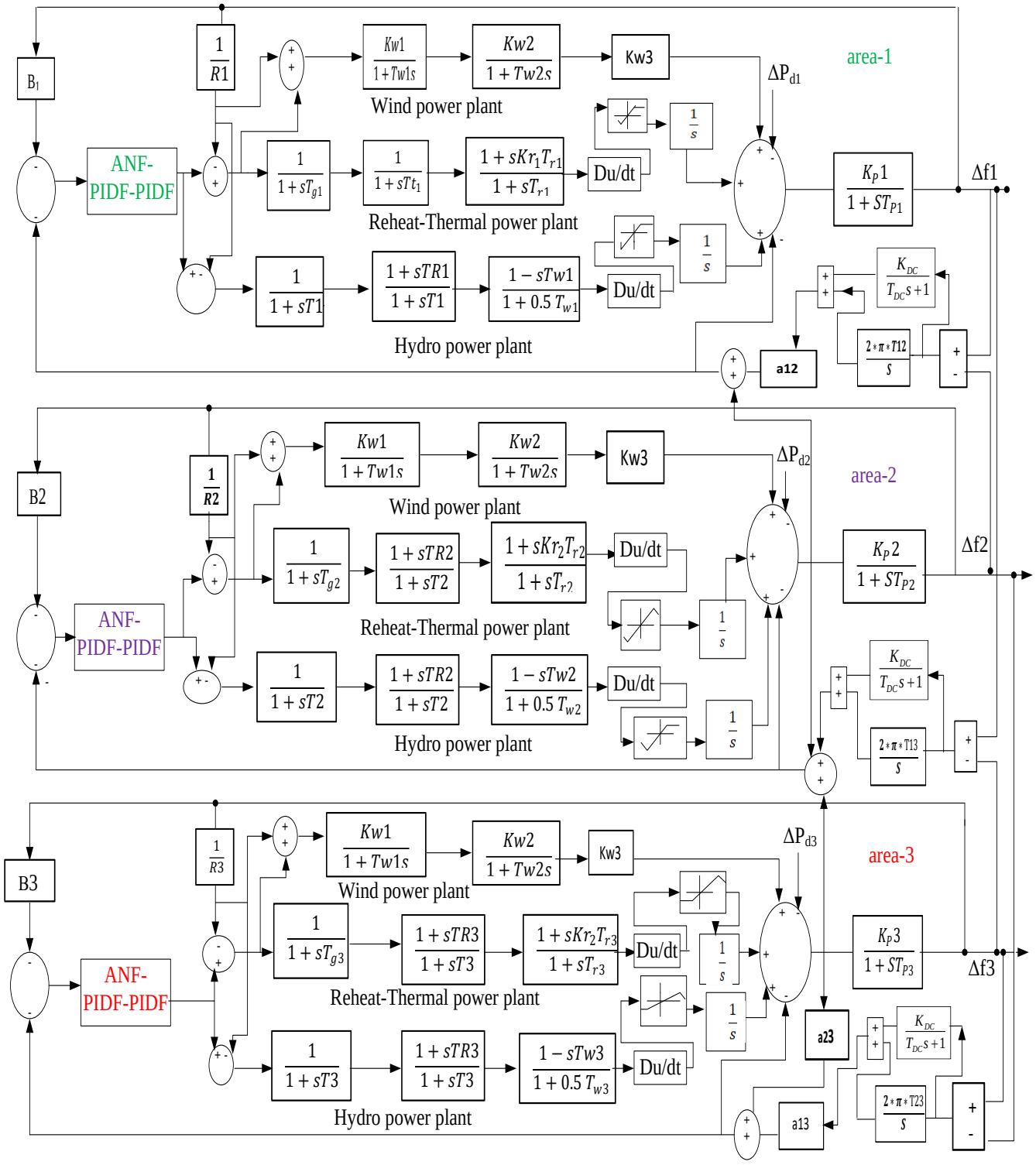

Figure 3. Three unequal area function models of AGC hybrid power systems under investigation

2.2 Systems Investigated

Figure 3 illustrates a block diagram of the system under investigation. Traditional interconnected power system (IPS) has three areas with unequal capacity, namely P_{r1}=2000 MW, P_{r2}=6000 MW, and P_{r3}=12000 MW, with wind power plants in areas 1, 2, and 3, as well as a re-heated thermal power plant (RTPP) and hydropower plant (HPP) acting as traditional power sources. The three unequal areas' various parameter per-unit values are compared on a respective basis. Therefore, a parameter a_{12} = - P_{r1}/P_{r2}, a_{23} = -

Preprints (www.preprints.org) | NOT PEER-REVIEWED | Posted: 22 November 2022 doi:10.20944/preprints202211.0422.v1

P_{r2}/P_{r3}, and $a_{13} = -P_{r1}/P_{r3}$ are taken into consideration in the three-area system when modeling interconnected areas with varying capabilities. In the system considered, speed regulation parameters of $R_i = 4$ % (2.4 Hz/pu) and frequency bias parameters of $B_i = \beta_i = 0.425$ are chosen. In practice, the rate of change in generating power has a maximum and a minimum value. In this study, the authors considered appropriate generation rate constraints (GRC) for each area for thermal and hydropower plants but not for wind power plants. The GRC restriction value of 3% per/min took into account the re-heating thermal system and hydro system 270% per/min for the rising system generation and 360% for lowering generation [26]. This work's mathematical model of different plants assumed for an interconnected power system was adapted from. The Appendix contains their nominal parameter values. Each subsystem is described in detail in the section that follows. A multi-area power system's frequency is within reasonable bounds, and the tie line exchange power should maintain within reasonable bounds. In addition, each location must absorb its load schedule [34]. In most cases, this is accomplished in the additional feedback loop by having to add a tie-line power variation to the system frequency deviation. It is known as tie-line bias control. For area 1, the area control error (ACE) is a combination of frequency and tie-line power variations. In any domain, Eq. (30) could be expressed as ACE. The dynamic system performance is evaluated for all areas using 1% step load perturbation (SLP).

$$ACE_i = \sum_{j=1}^{n} \Delta P_{ij} + K_i \Delta\omega \tag{30}$$

Where K_i is known as area bias, it controls how much interaction occurs when one region is disturbed by another. When the gains K_i value is selected to equal the frequency bias factor of that area B_i, which Eq. (31) identifies, a steady-state performance is attained.

$$B_i = \frac{1}{Ri} + D_i \tag{31}$$

Where B_i, is frequency bias factor of area i, R_i governor speed regulation parameter of area i.

When a steady state is attained, this control can immediately modify the reference power set point (ΔP_{ref}).

2.3. The proposed optimal Adaptive Neuro-Fuzzy-PIDF-PIDF controller (NF-PIDF-PIDF) modeling

2.3.1. Fuzzy logic controller (FLC)

In 1965, FLC theory was introduced as a theoretical idea that advances conventional control theories. FLC is a crucial instrument for mathematical methods for resolving power system issues. In order to increase the reliability and resilience of power system control, a sizable body of literature has been documented on FLC applications. A robust fuzzy logic-based tuning strategy for AGC regulators in a multi-area power grid is described, along with a design process and numerical validation. However, extreme caution must be exercised when designing, tweaking, and deploying these systems. FLC includes fuzzification, rule-based fuzzy inference systems, and Defuzzification [42].

Fuzzification changes a crisp quantity (set) into a fuzzy quantity (set). It is necessary to admit the utter no determinism and uncertainty of the different known crisp and deterministic quantities. This uncertainty may have developed due to fuzziness and imprecision, leading to the variables' capacity to be represented by a membership function. The rule base explains the entire control scheme and is essentially an if-then rule [43]. The Membership functions and rule foundation must be tuned to create a well-structured Fuzzy controller. Because these rules have been converted into fuzzy forms, using the fuzzy inference system is impractical. This study used a well-known "center of gravity" Defuzzification approach, and Mamdani FIS was used to increase the firing power of the

Preprints (www.preprints.org) | NOT PEER-REVIEWED | Posted: 22 November 2022 doi:10.20944/preprints202211.0422.v1

rule base [32]. Additionally, seven membership functions with 7*7=49 criteria were considered in the earlier literature on AGC for the fuzzy controller design. However, it is insufficient to optimize the heavy-loading power system. The authors updated the eleven membership functions to adapt to the intricate dynamic framework, resulting in 11*11=121 Rules.

Defuzzification is converting fuzzy values into crisp values that plants can use. The Fuzzy logic controller takes two Scaling Factors, K_{i1} and K_{i2}, as inputs and outputs, K_{o3}. An equal representation of input and output membership functions is required to ensure exceptional computing performance and memory utilization [44]. According to the literature review, triangular membership functions are preferred because they are simple to develop in real-time applications, consume less memory, and are simple to run through a fuzzy interfacing system (FIS). As a result, eleven MFs are considered for both outputs and inputs. All MFs have a value between -1 and 1, [45- 48]. Mamdani, obtain the value for each membership function output. The logic of the fuzzy interface system generates. The Mamdani Fuzzy interface system logic generates the output from each rule basis. PV stands for "positive very high," PL for "positive large," PB for "positive big," PM for "positive medium," PS for "positive small," ZR for "zero," NS for "negative small," NM for "negative medium," NB for "negative big," NL for "negative large," and NV for "negative very high" (negative very high). Figure 4 depicts the basic block diagram of fuzzy logic controller. The range of all membership operations is from -1 to 1, as illustrated in Figure. 5 (a)-(c).

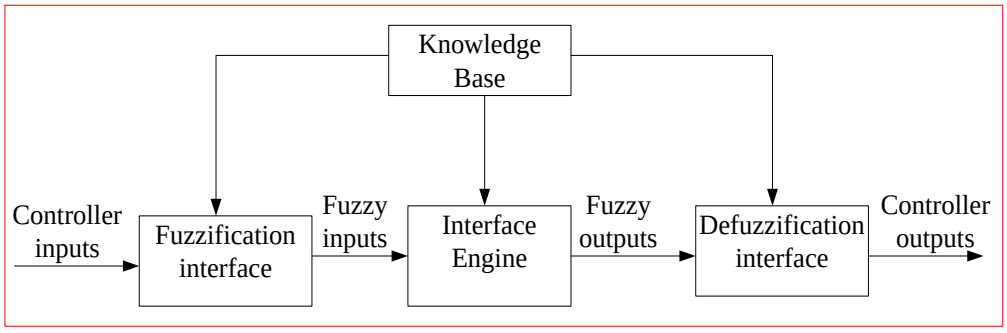

Figure 4. Block diagram of fuzzy logic controller

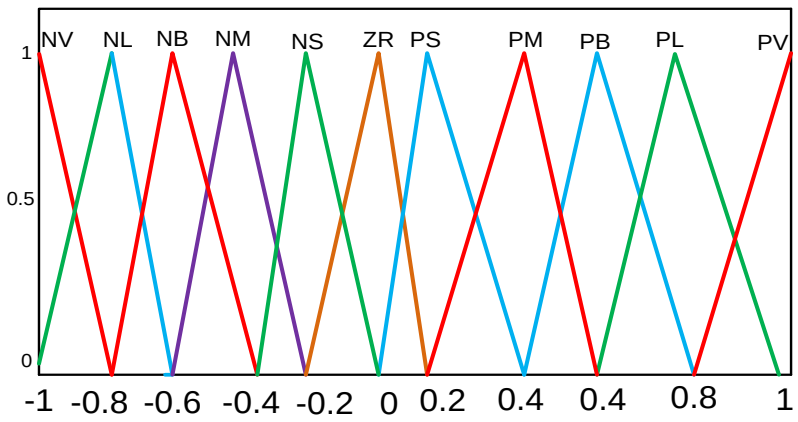

(a)

Preprints (www.preprints.org) | NOT PEER-REVIEWED | Posted: 22 November 2022 doi:10.20944/preprints202211.0422.v1

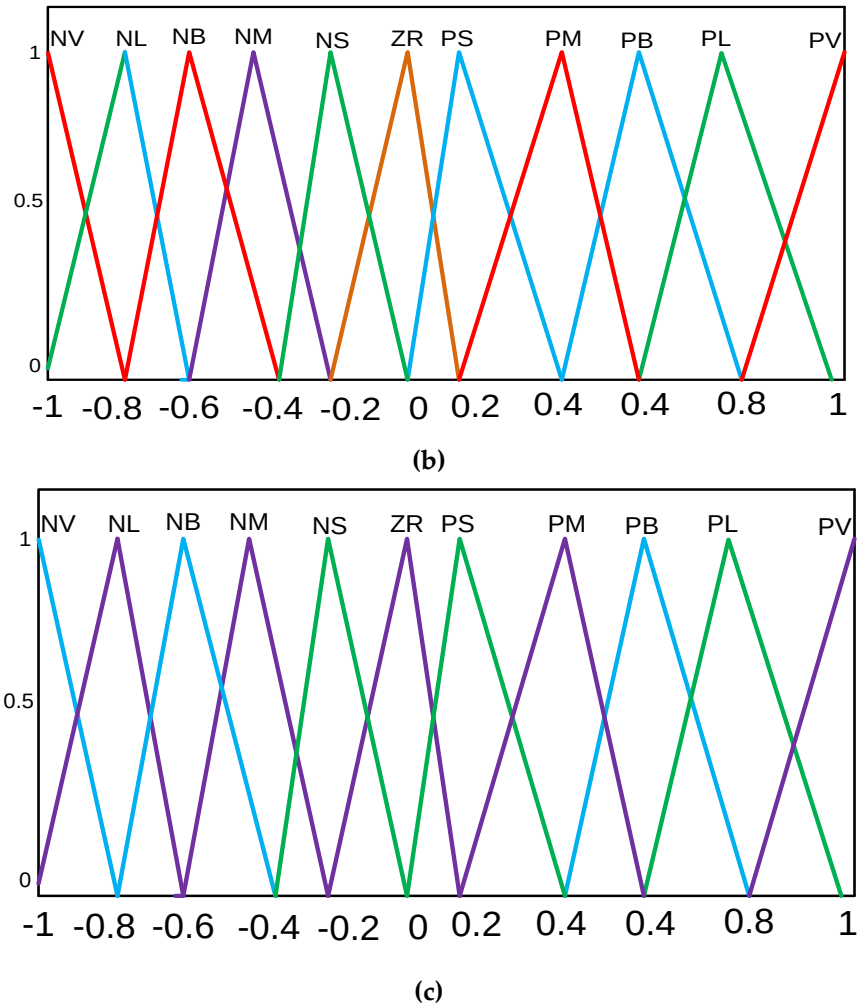

Figure 5. Fuzzy logic control membership functions. (a) Error input signal (e), (b) Error derivative input signal (de), (c) error output signal (u)

2.3.2. Artificial Neural Network (ANN)

Artificial neural networks' best approximation of arbitrary non-linear functions and application to parallel processing and multivariable systems are particularly interesting to researchers. A neural network may learn in a sophisticated multi-layer network, mimicking the human brain, and respond intelligently. The ANN in deep learning algorithms used with supervised and unsupervised learning methods can have a variety of topologies. Additionally, ANN's recently developed reinforcement learning algorithms are gaining popularity in practical applications. Researchers' offer and use ANN schemes throughout AGC systems' building [49]. An ANN-based AGC for a three-area integrated power grid network is proposed to achieve the minimum acceptable regulation in the area frequency and eliminate the disturbance's effect during heavy loading conditions and line disturbances [50].

Artificial intelligence techniques use the human nervous system's ability to adapt and learn. An artificial neural network is a structure of artificial neurons used in artificial intelligence. The ANN basic model is depicted in Figure.6. Neuron Structure comprises the following elements: x_p stands for Inputs, w_{kp} stands for Weights, p_{hi} (φ) stands for activation function, and out stands for output. The net input of the activation function is diminished using the threshold [43-50].

Preprints (www.preprints.org) | NOT PEER-REVIEWED | Posted: 22 November 2022 doi:10.20944/preprints202211.0422.v1

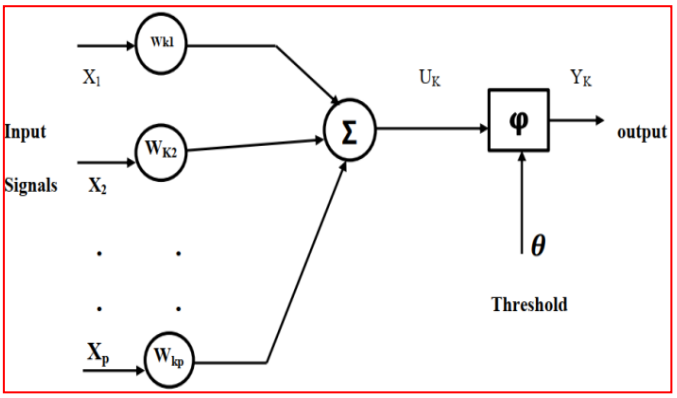

Figure 6. Non-linear model of a neuron

2.3.3. Adaptive Neuro-Fuzzy Inference System (ANFIS)

Adaptive Neuro-fuzzy inference is used to modify the membership function parameters of fuzzy inference systems of the Mamdani type (ANFIS). Using test data alters the structure of the inference system and assesses the tuned system's propensity for generalization. The ANFIS is one approach for constructing a fuzzy inference system given input/output data pairs. The fuzzy logic controller and neural network used in the ANFIS enable the controller to be self-tuning and adaptive. If we combine these two cutting-edge strategies, we will produce high-quality and quantity reasoning. The related FIS can track the input/output data with the help of this system's fuzzy logic capability, which can be used to adjust the membership function parameters. The parameters of the ANFIS model will be changed using the information collected from the FIS controller. It is essential to modify the typical neural network structure to build a fuzzy rule using neural networks [50].
Figure 7 depicts the block diagram of the hybrid neuro fuzzy controller. The architecture of this model is depicted in Figure. 8 and can be used to train and change the fuzzy interfaces system design uploaded to the ANFIS. The first layer's black circles represent the inputs, the second layer's white circles the input membership functions, the third layer's blue circles the rules, the fourth layer's white circles the output membership function, and the fifth layer's white circles the tuned output.

Fuzzification changes a crisp quantity (set) into a fuzzy quantity (set). It is necessary to admit the utter no determinism and uncertainty of the different known crisp and deterministic quantities. Defuzzification is converting fuzzy values into crisp values that plants can use. Fuzzy inference uses fuzzy logic to formulate the mapping from a given input to an output. The knowledge base is represented in rules, and Mamdani's most common rule structure involves linguistic variables. Hence, when dealing with multiple inputs-single output (MISO) systems. The knowledge base comprises two parts: a database and a rule base. The database contains information about domain boundaries, domain transformations, and fuzzy sets with corresponding linguistic terms. 126 The rule base contains linguistic control rules. Modern, sophisticated knowledge-based systems are robust because they integrate databases, knowledge bases, inference, and conventional numerical and algorithmic approaches effectively and efficiently. The authors provide an overview of handling imprecision in these three domains using fuzzy logic in general and fuzzy query, fuzzy rule-based inference, and fuzzy optimization in particular. This is in conjunction with soft computing and new technology requirements. Imprecise data transfer, cooperative techniques, and recurrent utilization integration problems are also addressed.

Preprints (www.preprints.org) | NOT PEER-REVIEWED | Posted: 22 November 2022 doi:10.20944/preprints202211.0422.v1

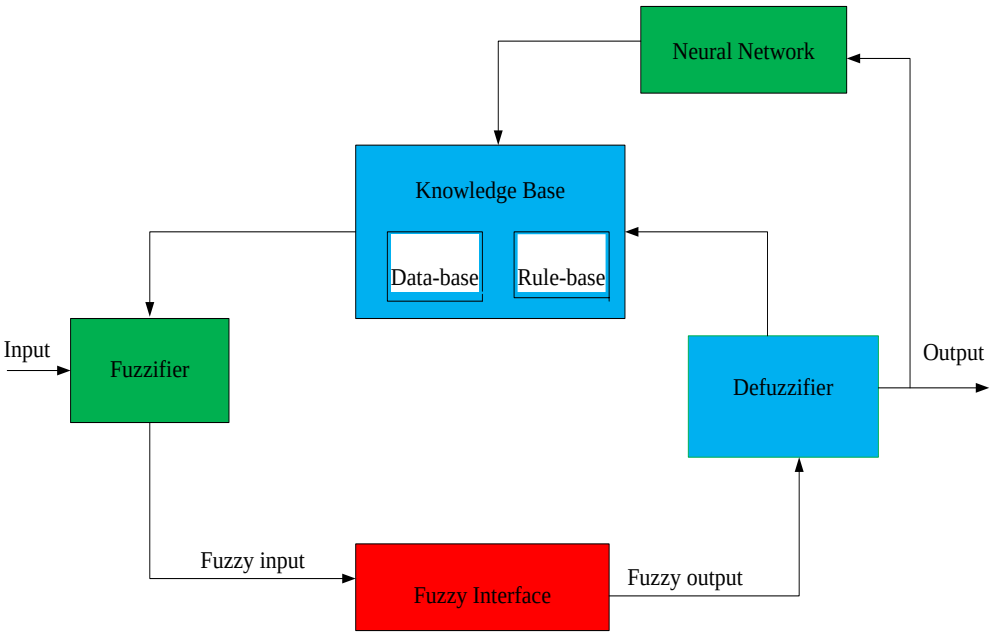

Figure 7. Block diagram of hybrid Neuro-fuzzy controller

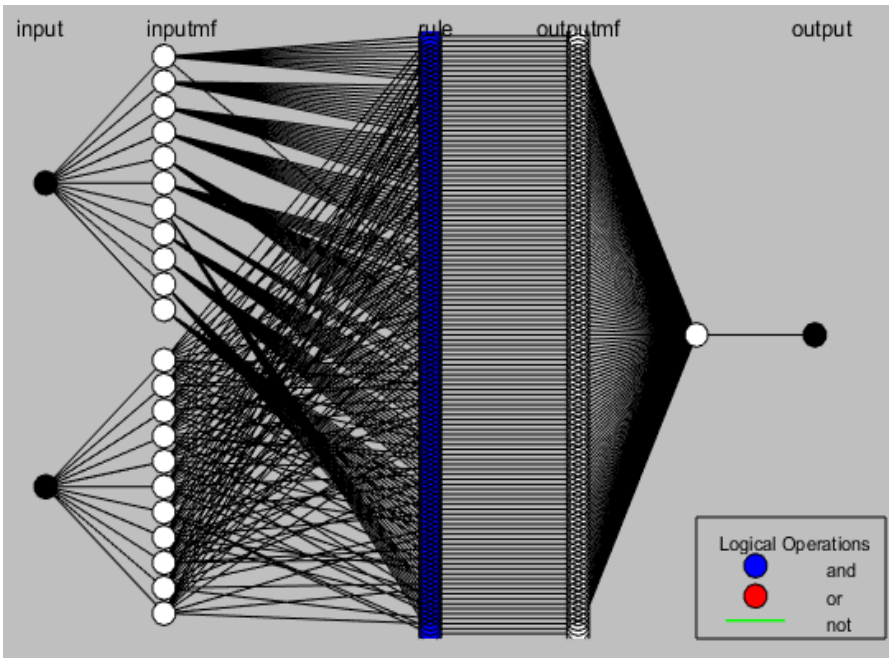

Figure 8. Adaptive Neuro-Fuzzy interface system structure

The adaptive network can be converted into traditional feed-forward neural network architecture. This suggested network performs similarly to the Mamdani fuzzy controllers' adaptive network simulator. A 2-input ANFIS with 121 rules is depicted in Figure 8. Each input has a corresponding set of eleven membership functions, resulting in 121 subspaces subdivided according to fuzzy if-then rules. The consequent part of a rule specifies the output within the fuzzy subspace defined by the premise. The function family listed below corresponds to the node functions in the same layer. The first layer is the input layer. Crisp external signals are transmitted to Layer 2 by neurons in this layer. The second layer is the fuzzification layer. Fuzzification is carried by neurons in this layer using the triangle membership function. The third layer is the ruling layer. A single fuzzy rule of the Mamdani type corresponds to each neuron in this layer. A rule neuron calculates the rule's firing strength using input from the corresponding fuzzification neurons. The operator product in an ANFIS assesses the conjunction of the rule antecedents. The fourth layer is the normalization layer. Each neuron in this layer processes information from every neuron in the rule layer to determine the normalized firing strength of a specific rule. The ratio of a given rule's firing

Preprints (www.preprints.org) | NOT PEER-REVIEWED | Posted: 22 November 2022 doi:10.20944/preprints202211.0422.v1

strength to the total firing strength of all rules is known as the normalized firing strength. It shows how a particular rule affected the result. The fifth layer is the Defuzzification layer. This layer's normalization neurons serve as the initial inputs for each neuron and are coupled to them. Here, the maximum membership value of each function in the output is weighted, forming the weighted average Defuzzification approach. Layer 6 is represented by the neuron that calculates the sum of outputs of all Defuzzification neurons and produces the overall ANFIS output.

2.3.4. Cascaded Proportional-Integration-Derivative with Filter Coefficient (PIDF-PIDF) Controller

The Proportional-Integral-Derivative with filter coefficient (PIDF) control is the most common control algorithm used in industry and has been universally accepted in industrial control. The popularity of PID controllers can be attributed partly to their robust performance in a wide range of operating conditions and partly to their functional simplicity, which allows engineers to operate them in a simple, straightforward manner. However, the performances of conventional controllers are not so promising in a higher-order system with non-linearity. Most of the time, classical techniques diverge from optimal solutions, are time-consuming, and suffer from premature convergence.

Improved stability and quicker controller response can be attained using conventional PID control. However, due to the derivative mode, the plant receives excessively high levels of meaningful control inputs. The noise already presents in the control signals is the primary culprit in this issue. The injected noise is removed by including a filtering portion in the derivative part. The noise chattering can be decreased by fine-tuning the pole. Therefore, in the cascaded controller, the PIDF-PIDF is chosen.

To enhance the effectiveness of the control, it combines the PID-PID with the derivative filter. The developed controller's primary objective is to control the frequency response in each area during load fluctuations, renewable energy source changes, and unpredictable power system conditions. To reduce the disturbance effects that enter the secondary loop from the primary loop using the cascaded structure of AGC. As a result, it can deliver more incredible performance compared to architectures with a single control loop. They can lessen the effects of gain changes on system performance, which is an additional benefit.

$$G_C(s) = K_P + \frac{K_I}{s} + K_D s\left(\frac{1}{1+\frac{s}{N}}\right) \tag{32}$$

The output of one control serves as an input set point for the other control in the cascaded control structure being used. The set point for the second stage is provided by the ANFIS, which is used as the primary external control loop or master controller. The secondary controller of the slave controller, which is part of the inner control loop, uses the PIDF-PIDF. Figure.9 depicts the generalized cascade controller structure. Where c(s) is the adaptive Neuro-fuzzy controller, c(s) is the PIDF-PIDF controller, g(s) is the first-order transfer function of the system, and g(s) is the power system's first-order transfer faction.

The output of one control serves as an input set point for the other control in the cascaded control structure being used. The set point for the second stage is provided by the ANFIS, which is used as the primary external control loop or master controller. The secondary controller of the slave controller, which is part of the inner control loop, uses the ANF-PIDF-PIDF. Figure. 10 depict the physical layout of the proposed cascaded ANF-PIDF-PIDF controller [48-51].

The cascade control can be thought of as a feedback-combining method. In this control method, the inner loop controller would get its set point from an outer-loop control. So there would be two controllers in this control system, and the output of one is the input of the other. As a result, in this controller, the secondary controller works in tandem with the primary controller to improve control of the primary process variable.

Preprints (www.preprints.org) | NOT PEER-REVIEWED | Posted: 22 November 2022 doi:10.20944/preprints202211.0422.v1

A second measurement and secondary feedback would be included in the cascade loop. A cascade control system would consist of two controllers, with the output of one driving the set point of the other. This structure has multiple loops, and the principal output of the controller in the outer loop corresponds to the controller's set point in the inner loop. Because the process is divided into two and one process variable will be changed, two controllers are utilized in cascade control [51].

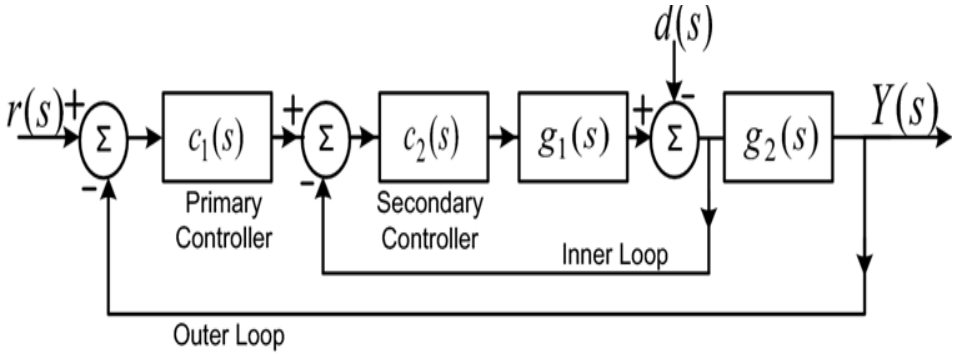

Figure 9. Generalized cascade controller structure

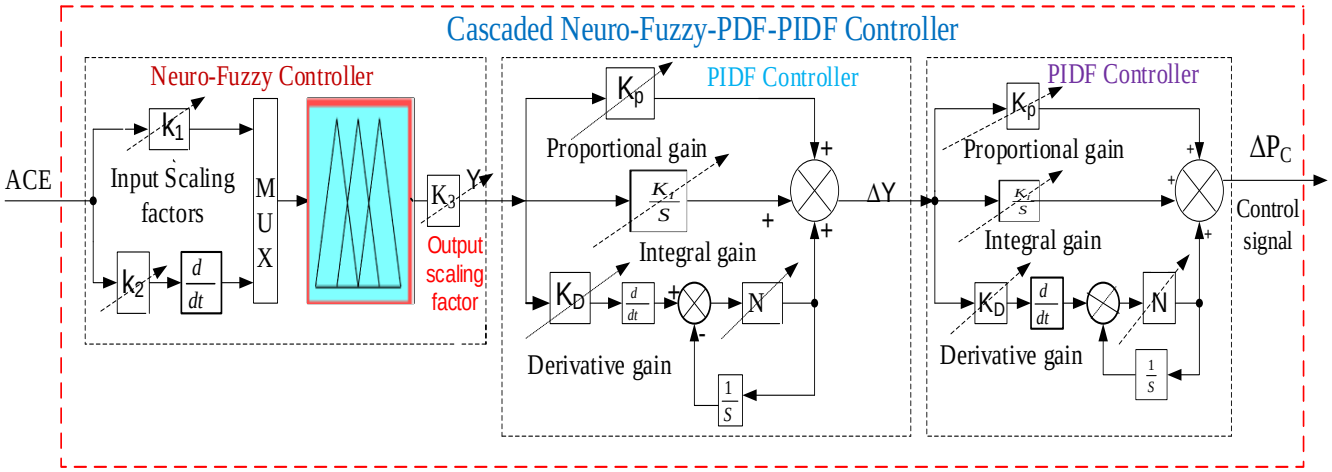

Figure 10. Block diagram of the proposed control using hybrid Neuro-Fuzzy-PIDN controller for AGC

2.4. Skill Optimization Algorithm

Metaheuristic algorithms are widely used in solving optimization problems. This paper proposed a recent metaheuristic algorithm called the Skill optimization Algorithm (SOA) to solve optimization problems. The real inspiration for designing SOA is human efforts to acquire and improve skills [52]. To choose the best response, the SOA starts by creating a random population of different strings. The fitness value of each agent for the present population's next generation is determined at each stage. Fitness is the encoded value of the objective function's solution with appropriate performance indices, which must be optimized. The procedure is repeated until the ideal and worldwide answer has been identified. The SOA is used to determine the values of the best PIDN gain parameters, including fuzzy scaling factors (K_1, K_2, and K_3) controllers for AGC and K_P, K_I, K_D, and N. Figure.11. depicts the SOA flow chart for determining the appropriate optimization parameter values [47-48]. Before creating the Neuro-fuzzy logic-based PIDN controller, selecting the target function with the requirements and limits is more important. The benchmarks determine which goal function is used to optimize the controller gain settings. Performance criteria are assessed using time-domain specifications for peak overshoots undershoots, settling time, and steady-state error.

Preprints (www.preprints.org) | NOT PEER-REVIEWED | Posted: 22 November 2022 doi:10.20944/preprints202211.0422.v1

The number of search agents (n) = 30, the population size (n) = 100, the problem dimension (d) = 21, the damping coefficient (d) = 0.7, and the maximum number of iterations (N) = 50 are all taken into account in this simulation. The constraint in equation (37) is applied to the cost function values in this optimization.

2.4.1. The Proposed Optimization Process

The optimization procedure is driven by minimizing the fitness function that has been selected. The frequency deviations in area 1, 2 and 3, (ΔF_1, ΔF_2, ΔF_3), and the variation in the tie-line power between the three areas ($Ptie_{12}$, $Ptie_{23}$, and $Ptie_{13}$) are the six key metrics for the optimization process. Due to the inclusion of p.u. measurements, the objective function in the suggested optimization approach contains all six measures without weighing considerations. The suggested optimization procedure will make use of four primary representations of objective functions.
The frequency and tie-line power deviations were minimized in the suggested optimization technique in order to estimate the aforementioned objective functions. Additionally, the measures are applied during simulations while considering the various current constraints. The two areas' targeted control objectives and the four objective functions can be described as follows [55]:

$$ISE = \left(\int \Delta f_1^{\,2} + \Delta f_2^{\,2} + \Delta f_3^{\,2} + \Delta p_{tie12}^{\,2} + \Delta p_{tie23}^{\,2} + \Delta p_{tie13}^{\,2}\right)dt \quad (33)$$

$$ITSE = \left(\int \Delta f_1^{\,2} + \Delta f_2^{\,2} + \Delta f_3^{\,2} + \Delta p_{tie12}^{\,2} + \Delta p_{tie23}^{\,2} + \Delta p_{tie13}^{\,2}\right) t.\,dt \quad (34)$$

$$IAE = \left(\int abs\,(\Delta f_1^{\,2} + \Delta f_2^{\,2} + \Delta f_3^{\,2} + \Delta p_{tie12}^{\,2} + \Delta p_{tie23}^{\,2} + \Delta p_{tie13}^{\,2})\right)dt \quad (35)$$

$$ITAE = \left(\int abs(\Delta f_1^{\,2} + \Delta f_2^{\,2} + \Delta f_3^{\,2} + \Delta p_{tie12}^{\,2} + \Delta p_{tie23}^{\,2} + \Delta p_{tie13}^{\,2})\right) t.\,dt \quad (36)$$

Figure.9 depicts the essential steps of the SOA-based parameter tuning for the proposed controller, with the different parameters in areas 1, 2 and 3. The following is an expression for the control parameters' considered limits: Under the following constraints, skill optimization algorithms are used to tune controller parameters [56].

$$\left.\begin{array}{l} Kp,min \le Kp \le Kp,max \\ Ki,min \le Ki \le Ki,max \\ Kd,min \le Kd \le Kd,max \\ Nmin \le N \le Nmax \\ K1,min \le K1 \le k1,max \\ K2,min \le K2 \le k2,max \\ K3,min \le K3 \le K3,max \end{array}\right\} \quad (37)$$

Preprints (www.preprints.org) | NOT PEER-REVIEWED | Posted: 22 November 2022 doi:10.20944/preprints202211.0422.v1

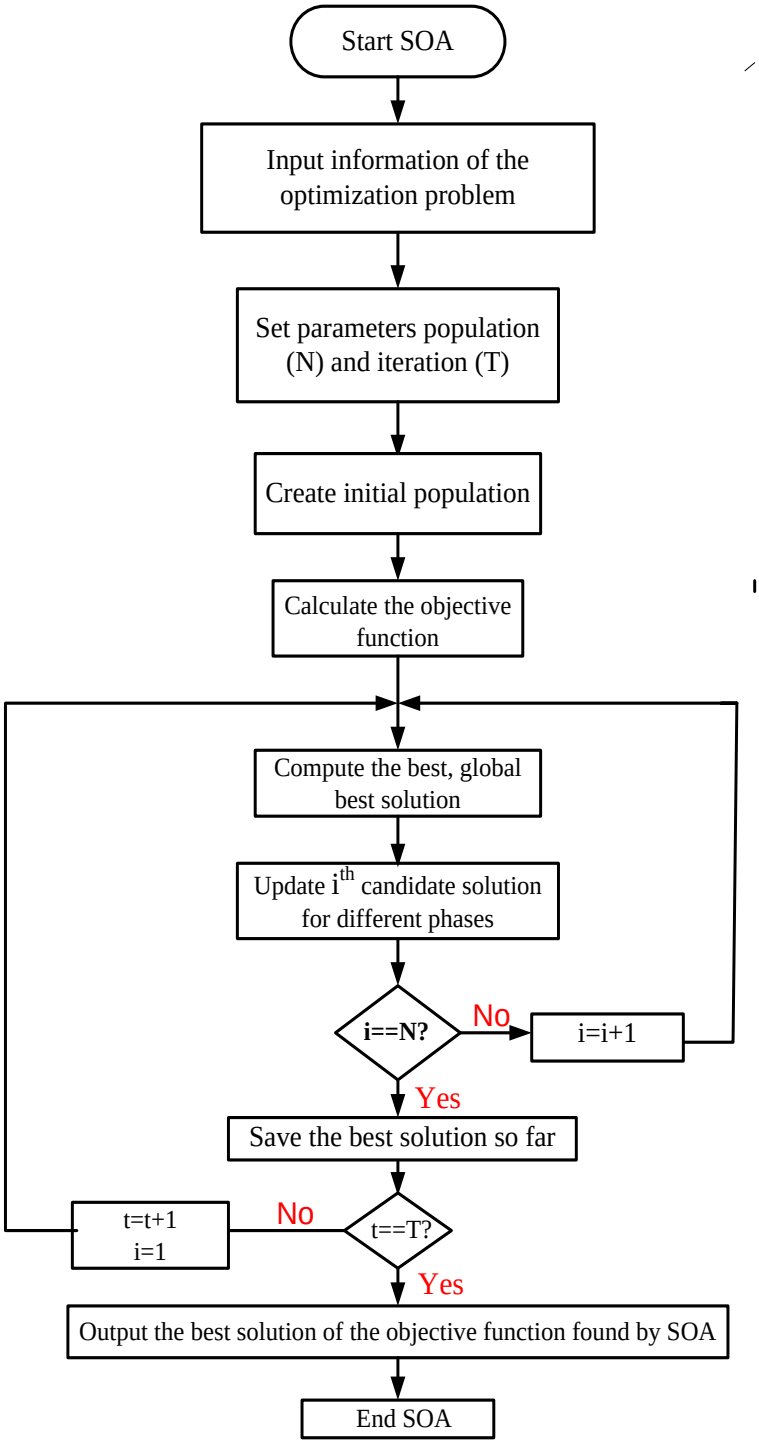

Figure.11. The flow chart of Skill Optimization Algorithm

The SOA is a population-based method, and its participants are actual individuals who are continuously striving to increase their knowledge and skills. In actuality, members of the SOA population are candidates for solving the optimization issue at hand. Based on the positions of these members in the search space, the values of the problem decision variables may be derived. The first placements of SOA members are decided by a random method at the start of the algorithm. A mathematical model of the SOA population may be developed using a matrix (Eq. 32)

Preprints (www.preprints.org) | NOT PEER-REVIEWED | Posted: 22 November 2022 doi:10.20944/preprints202211.0422.v1

$$X = \begin{bmatrix} X_1 \\ \vdots \\ X_i \\ \vdots \\ X_N \end{bmatrix} = \begin{bmatrix} x_{1,1} & \cdots & x_{1,d} & \cdots & x_{1,m} \\ \vdots & \ddots & \vdots & \ddots & \vdots \\ x_{i,1} & \cdots & x_{i,d} & \cdots & x_{i,m} \\ \vdots & \ddots & \vdots & \ddots & \vdots \\ x_{N,1} & \cdots & x_{N,d} & \cdots & x_{N,m} \end{bmatrix} \quad (32)$$

In this case, X is the population matrix for the SOA, X_i is the ith candidate solution, x_i, d is the value of the d^{th} variable that was suggested by the i^{th} population member, N is the number of members of the SOA, and m is the number of variables.

Each member of the population has the potential to contribute to the issue's resolution. In other words, a value for the target function is determined by putting each component into the corresponding variable in the problem.

$$F = \begin{bmatrix} F_1 \\ \vdots \\ F_i \\ \vdots \\ F_N \end{bmatrix}_{N\times 1} = \begin{bmatrix} F(X_1) \\ \vdots \\ F(X_i) \\ \vdots \\ F(X_N) \end{bmatrix}_{N\times 1} \quad (33)$$

The target function values can be formally described using a vector according to Eq (33). F is a vector holding all objective function values, and F_i is the i^{th} candidate solution's objective function value. The best objective function value indicates the best member, whereas the worst value identifies the worst member. Since the goal function and population are modified on each iteration, the best and worst members of the population also vary.

SOA's population is updated by exploration and exploitation. In the exploring phase, you'll imitate learning from a pro. During the exploitation phase, you'll emulate individual users' skill improvement. The update process in SOA design involves two phases: exploration and exploitation. Exploration is a global search, while exploitation is a local search. During the exploratory phase, SOA members followed the instructions of other members rather than following the best member. This increases the algorithm's exploration capability, allowing it to better scan the search space and find the optimum spot. In the exploitation phase, the algorithm converges to improved likely solutions owing to local search near each population member.

5.1 The First Phase: Learning from Experienced Individuals (Exploration)

During the initial phase, each member of the SOA acquires a talent under the supervision of an expert member of the community. The value of an individual's objective function is exactly proportionate to his or her contribution to the population as a whole. An SOA member is considered to have an expert member when that member's conditions are assessed to be superior to those of the other members based on the value of the objective function. If a member of the SOA has a higher objective function value than any other member of the SOA, then the members with the highest objective function values are included in the "experts set" for that member. After being selected at random, one of these individuals will act as a mentor to the individual in question. Therefore, the chosen specialist to lead the SOA member may not always be the best selection. In reality, the best potential solution is a non-rotating member of the ex-experts set that applies to all SOA members. Learning the skill, which refers to the algorithm's capacity for both global search and exploration, directs the population to various locations inside the search space. This is the expert member's responsibility. If the new location estimated for each member of the population increases the goal function's value, it may be deemed ac-

Preprints (www.preprints.org) | NOT PEER-REVIEWED | Posted: 22 November 2022 doi:10.20944/preprints202211.0422.v1

ceptable. Consequently, the first phase of the update may be characterised using Equations (34) and (35) in line with the previously given concepts.

$$X_i^{P1}: X_{i,d}^{P1} = x_{i,d} + r \times \left(E_{i,d} - I \times x_{i,d}\right), E_i = X_k, \tag{34}$$

Where $F_k < F_i$ and k is randomly selected from {1,2,…,N}, k≠ i

$$X_i = \begin{cases} X_i^{P1}, & F_i^{P1} < F_i \\ X_i, else \end{cases} \tag{35}$$

Here, X^{P1} is the newly calculated status of the i^{th} candidate solution based on the first phase, x_{P1} is its I i,d d^{th} dimension, F^{P1} is the value of its objective function, E_i is the expert who has been chosen to guide and train the i^{th} member of the population, $E_{i,d}$ denotes its d^{th} dimension, r is a random number in the range [0 1], and I is a random number that is chosen at random from

5.2 The second phase focuses on improving one's skills via individual effort and practise (Exploitation)

During the second phase, every member of the population engages in autonomous study and practise to further enhance the skills acquired in the previous phase. This notion is modelled as local search in SOA in order to increase exploitation such that each member in the vicinity of its position seeks better circumstances to increase the value of its goal function. This is done with the intention of increasing exploitation as a whole (which indicates the level of skill). Similar to the previous step, the newly computed location in this phase is deemed acceptable if it increases the value of the objective function. Eqs. (3) and (367) are utilised to offer a mathematical representation of the ideas

$$X_i^{P2}: x_{i,d}^{P2} = \begin{cases} x_{i,d} + \frac{1-2r}{t} \times x_{i,d}, r < 0.5 \\ x_{i,d} + \frac{lb_{j+r(ub_j - lb_j)}}{t} \times x_{i,d}, else \end{cases} \tag{36}$$

$$X_i = \begin{cases} X_i^{P1}, & F_i^{P1} < F_i \\ X_i, else \end{cases} \tag{37}$$

Here, X^{P2} denotes the newly computed status of the ith candidate solution based on the second phase, x^{P2} denotes its d^{th} dimension, F^{P2} denotes the value of its objective function, t denotes the iteration counter, and lb_j and ub_j denote the lower and upper bounds of the j^{th} variable, respectively.

5.3 The Sequential Object Architecture's Repetition Process

After all SOA members have been brought up to date in accordance with the first and second phases, the first iteration of SOA is complete. The algorithm will then proceed to the next iteration, at which point the updating procedure will be carried out in line with Equations (33) to (37). When the SOA has been fully implemented, the output will include the optimal solution. Figure 5 displays the flowchart for the SOA.

Table2 displays the mean value of the assessment findings of Unimodal functions of various techniques compared to SOA, as presented in [46]. In terms of optimization, it is evident from the mean values of evaluation results for unimodal functions that SOA is better to any other approach. Multimodal functions have a comparable pattern. In Table 3, the mean values for unimodal functions F1 through F4 demonstrating the superiority of SOA are provided, although a similar pattern is observed for higher levels of function beyond F4.

Preprints (www.preprints.org) | NOT PEER-REVIEWED | Posted: 22 November 2022 doi:10.20944/preprints202211.0422.v1

Table 2 : Mean values of Evaluation results of Unimodal functions

	GA	PSO	GSA	TLBO	GWO	MVO	WOA	TSA	MPA	RFO	SOA
F1	21.26981	0.00051	7.68E-17	4.29E-61	1.3E-100	0.207125	6.5E-82	3.21E-82	5.99E-86	6.46E-84	0
F2	1.569531	0.591161	3.95E-08	4.47E-32	1.8E-58	0.300354	2.2E-175	1.82E-48	2.67E-47	6.78E-46	4.6E-191
F3	2081.245	1393.67	185.0622	1.03E-19	6.47E-29	21.44854	6629.856	3.65E-21	7.73E-23	4.67E-58	0
F4	2.69652	4.39557	1.05E-08	3.98E-25	9.73E-25	0.628421	35.21117	1.01E-05	1.23E-32	1.34E-35	1.9E-181

2.4.2. Implementation of AGC scheme

The objective function must be carefully chosen for the controller to operate at its best. AGC's (Δf_i) and ΔP_{tie} goals enhance post-disturbance system responsiveness. In comparison; an ISE-tuned controller can generate a strong control signal that could be hazardous in the event of an unexpected imbalance. A smaller initial weight can be offered since the error signal generated at the time of the load imbalance has a larger magnitude. While ITAE functions, which check the system's transient response, can severely punish errors that happen late. Additionally, ISE and ITSE offer outstanding step responses and can settle more quickly due to the greater weight given to time parameters. Since ISE provides the response with the least amount of oscillation and overshoot [53].

The SOA technique covered in the previous part is used in AGC, and the procedures are carried out under the flowchart in Figure. 10. Here, a population size of 100 and a maximum number of iterations of 50 have been taken into account. The outer and inner loops for the thermal, hydro, and wind power sources are the primary controller parameters for the cascaded ANF-PIDF-PIDF controller. Table.3 shows the comparative performance for different indices criteria considering various optimization techniques such as SOA, PSO, and GA with the proposed controller. The results show that the SOA technique-based present controller performs better than the GA and PSO technique-based present controller when all four performance indices ISE, IAE, ITSE, and ITAE are considered. Figure.12 clearly reveals that the integral squared error (ISE) is a better performance index than others [57-59].

Table3.Comparative performance for different indices criteria

Controller with techniques	**Objective function**			
	ISE $(\mathbf{x10^{-5}})$	**ITSE** $(\mathbf{x10^{-3}})$	**ITAE** $(\mathbf{x10^{-2}})$	**IAE** $(\mathbf{x10^{-2}})$
SOA-ANF-PIDF-PIDF	**1.4770**	**1.575**	**2.939**	**1.148**
PSO-ANF-PIDF-PIDF	1.6670	1.7635	5.225	1.3750
GA-ANF-PIDF-PIDF	2.0690	1.9610	8.360	1.7270

Preprints (www.preprints.org) | NOT PEER-REVIEWED | Posted: 22 November 2022 doi:10.20944/preprints202211.0422.v1

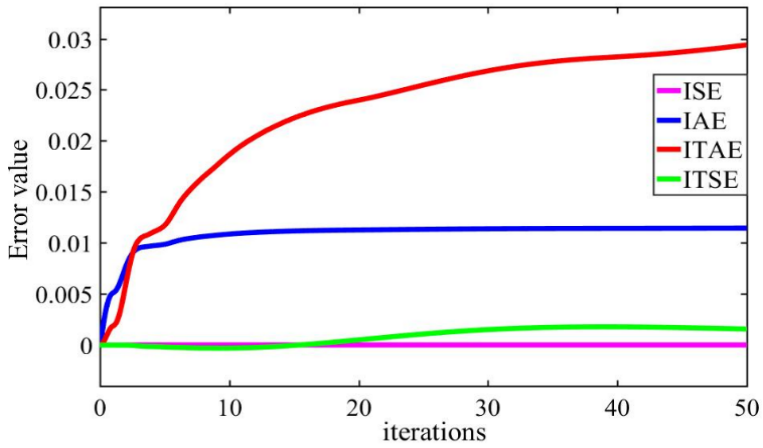

Figure.12. Various performance indices comparison considering proposed SOA

3. Results and Discussion

The AGC problems of three unequal-area interconnected power systems are considered with the linearity and non-linearity systems. A hybrid combination of adaptive Neuro-Fuzzy and cascaded PIDF is used to evaluate multi-area multi-source power systems' frequency and tie-line responses. The simulations were carried out with PIDF, PIDF-PIDF, and adaptive Neuro-Fuzzy, controllers, and the results have been compared. Table 4 shows optimized controller gains and scaling factor values of three unequal areas of the hydro-thermal system incorporating wind energy using Skill Optimization Algorithm and considering traditional PIDF cascaded PIDF, and optimal Neuro-Fuzzy cascaded PIDF controller We have shown the Scaling Factors -K_{pi}, K_{Ii} , K_{Di} as well as N_i for Area 1,Area 2 and Area 3 for six different cases . In the first case, the gains and scaling factors are obtained using a PIDF controller. In the Second case, they are obtained using a PIDF-PIDF controller. In the third case, they are obtained using an ANF-PIDF-PIDF controller. In the fourth case, they are obtained using a PIDF with GRC. In the fifth case, they are obtained with a cascaded PIDF with GRC. In the sixth case, they are obtained with an ANF-PIDF-PIDF with GRC. Through the results obtained, we can infer that system with a conventional PIDF controller performs poorly compared to a cascaded PIDF and the optimal Neuro-Fuzzy-cascaded PIDF controller performs even better than the cascaded PIDF controller[60]. For instance, the N_i for PIDF is 49.85,59.571 and 45.679 for Area 1,Area 2 and Area 3 respectively. The N_i for cascaded PIDF is 49.85,57.571 and 35.679 35.679 for the three areas respectively while it is even lower for ANF-PIDF-PIDF with 49.85,57.571, and 35.679 respectively for the three areas. This can also be noticed when the controllers are used with GRC. For instance, the N_i for PIDF with GRC is 96.06,97.7 and 98.97 for Area 1,Area 2 and Area 3 respectively. The Ni for cascaded PIDF with GRC is 69.85,57.571 and 55.679 for the three areas respectively while it is even lower for ANF-PIDF-PIDF with GRC with 75.11,72.57, and 47.034 respectively for the three areas.

Preprints (www.preprints.org) | NOT PEER-REVIEWED | Posted: 22 November 2022 doi:10.20944/preprints202211.0422.v1

Table.4: Optimized controller gains and scaling factors values of three unequal areas hydro-thermal system incorporating wind energy using Skill Optimization Algorithm

Controllers	Gains/scaling factors	Area-1	Area-2	Area-3
PIDF	K_{pi}^*	0.2062	0.1474	0.261
	K_{Ii}^*	0.1489	0.2467	0.2460
	K_{Di}^*	0.0878	0.2837	0.0762
	N_i^*	49.85	59.571	45.679
PIDF-PIDF	K_{pi}^*	0.1627	0.1374	0.251
	K_{Ii}^*	0.1389	0.2367	0.2560
	K_{Di}^*	0.0878	0.2737	0.0362
	N_i^*	49.85	57.571	35.679
ANF-PIDF-PIDF	K_{pi}^*	0.1627	0.1374	0.251
	K_{Ii}^*	0.1389	0.2367	0.2560
	K_{Di}^*	0.0378	0.2737	0.0362
	Ni*	49.85	57.571	35.679
	K_{1i}^*	0.224	0.1940	0.2696
	K_{2i}^*	0.195	0.0185	0.2085
	K_{3i}^*	0.20951	0.2825	0.1931
PIDF with GRC	K_{pi}^*	0.231	0.152	0.322
	K_{Ii}^*	0.282	0.291	0.0291
	K_{Di}^*	0.0062	0.0025	0.0212
	N_i^*	96.06	97.7	98.97
PIDF-PIDF with GRC	K_{pi}^*	0.6766	0.698	0.425
	K_{Ii}^*	0.442	0.1569	0.271
	K_{Di}^*	0.2486	0.0457	0.0995
	Ni*	69.85	57.571	55.679
ANF-PIDF-PIDF with GRC	K_{pi}^*	0.3093	0.2522	0.5966
	K_{Ii}^*	0.2735	0.552	0.3548
	K_{Di}^*	0.671	0.565	0.4452
	N_i^*	75.11	72.57	47.034
	K_{1i}^*	0.0324	0.4525	0.0948
	K_{2i}^*	1.19	1.02	1.095
	K_{3i}^*	0.0899	0.0978	0.0877

3.1. *System dynamics research using various controllers and modeling*

Figure.13. Shows that the dynamic responses comparison with various controllers with and without considering wind power plants (WPP).The optimum plant parameter for three areas of the power system is taken from Table 4. The results illustrate that the optimal Neuro-Fuzzy-PIDF-PIDF has an excellent dynamic response over the other controllers regarding settling time, overshoot and undershoot as illustrated in Table 5. 6 different frequency deviations are considered. The Undershoot, Overshoot and Settling time of 6 different cases of controllers – PIDF without wind, PIDF-PIDF without wind, ANF-PIDF-PIDF without wind, PIDF with wind, PIDF-PIDF with wind, ANF-PIDF-PIDF with wind are presented for each frequency deviation. In Figure 13. (a), the data are presented for the deviation in area 1 frequency. In figure 13. (b), the data are presented for the deviation in area 2 frequency. In figure 13. (c), the data are presented for the deviation in area 3 frequency. In figure 13. (d), the data are presented for the deviation in tie-line power connecting area 1 and area 2. In figure 13. (e), the data are presented for the deviation in tie-line power connecting area 2 and area 3. In figure 13. (f), the data are presented for the deviation in tie-line power connecting area 1 and area 3. In the cases, the load of the hydrothermal system is efficiently shared by integrating wind power plant units into hydrothermal units through parallel operation, which also considerably enhances the tie line power exchange from one area to another. Overall, it can be in-

Preprints (www.preprints.org) | NOT PEER-REVIEWED | Posted: 22 November 2022 doi:10.20944/preprints202211.0422.v1

ferred that the ANF-PIDF-PIDF performs way better than the PIDF-PIDF and PIDF controllers.

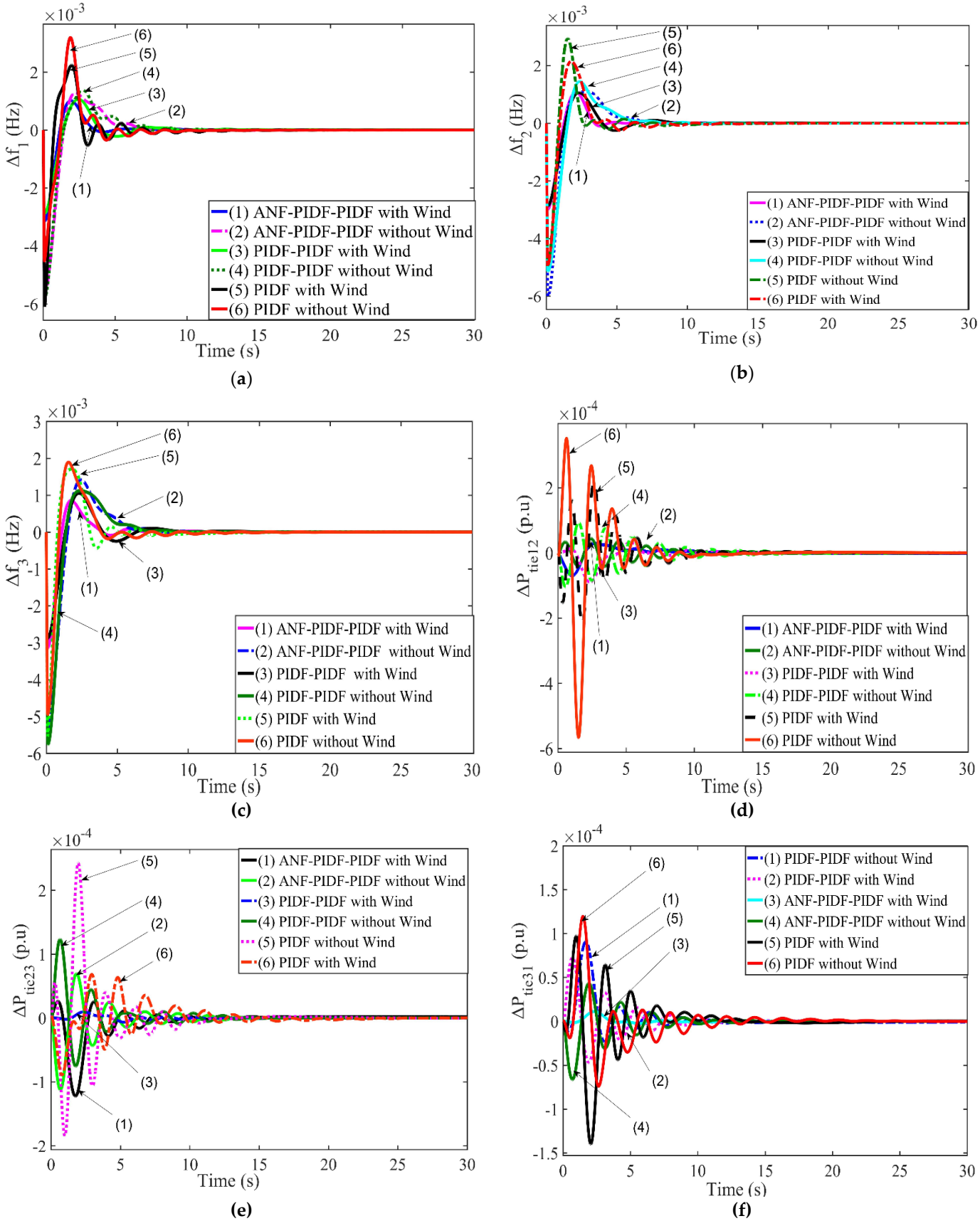

Figure.13. the dynamic responses comparison with various controllers with and without considering wind power plants. **(a)** deviation in area-1 frequency , (b) deviation in area-2 frequency, (c) deviation in area-3 frequency (d) deviation in tie line power connecting area-1 and area-2, (e) deviation in tie line power connecting area-2 and area-3, (f) deviation in tie line power connecting area-1 and area-3

Preprints (www.preprints.org) | NOT PEER-REVIEWED | Posted: 22 November 2022 doi:10.20944/preprints202211.0422.v1

The load of the hydrothermal system is efficiently shared by integrating wind power plant units into hydrothermal units through parallel operation, which also considerably enhances the tie line power exchange from one area to another. In comparison to the only PIDF controller, the percentage improvement in overshoot (OS) and settling time (T_S) of Δf_1 with the optimal adaptive NF-PIDF-PIDF controller is 69.81% and 48.87%, respectively. Similarly, the suggested adaptive NF-PIDF-PIDF controller improves overshoot (OS) and settling time (T_S) of Δf_2 by 67.65% and 25.47%, respectively, compared to the traditional PIDF controller. Similarly, Δf_3 improves overshoot (OS) and settling time (T_S) by 59% and 26.73%, respectively, compared to the traditional PIDF controller. In addition, as compared to the simple PIDF, classical PIDF controller, and adaptive NF-PIDF-PIDF controller improves ΔP_{tie12}; ΔP_{tie23} and ΔP_{tie13} overshoot (OS) and settling time (T_S) by (82.85%, 44.58%), (85.26%, 44.78%) and (58.34%, 26%) respectively. As a result of the investigation, as mentioned earlier, the SOA-based adaptive NF-PIDF-PIDF controller claims to provide significant improvements. Tables also show that the proposed controller performed better in terms of response. The proposed controller's settling time (ts) was frequently shorter than that of a PIDF controller. Furthermore, we discovered that the oscillation of the proposed controller is appropriate for load frequency management.

Table.5: Performance comparison PIDF, cascaded PIDF and ANF-PIDF-PIDF controllers with and without wind power plants

Control action	Controllers	Undershoot	Overshoot	T_S (s)
Δf_1 (Hz)	PIDF with wind	$-6.1x10^{-3}$	$2.24x10^{-3}$	15
	PIDF without wind	$-5.08x10^{-3}$	$3.19x10^{-3}$	16
	PIDF-PIDF with wind	$-2.88x10^{-3}$	$1.06x10^{-3}$	14
	PIDF-PIDF without wind	$-5.48x10^{-3}$	$1.29x10^{-3}$	14.5
	ANF-PIDF-PIDF with wind	$-3.17x10^{-3}$	$1.01x10^{-3}$	8.5
	ANF-PIDF-PIDF without wind	$-5.58x10^{-3}$	$1.3x10^{-3}$	13
Δf_2 (Hz)	PIDF with wind	$-4.9x10^{-3}$	$2.95x10^{-3}$	11.5
	PIDF without wind	$-5.08x10^{-3}$	$2.14x10^{-3}$	20
	PIDF-PIDF with wind	$-2.97x10^{-3}$	$1.15x10^{-3}$	12
	PIDF-PIDF without wind	$-5.18x10^{-3}$	$1.4x10^{-3}$	12.5
	ANF- PIDF-PIDF with wind	$-3.03x10^{-3}$	$1.1x10^{-3}$	10.5
	ANF- PIDF-PIDF without wind	$-6x10^{-3}$	$1.1x10^{-3}$	12
Δf_3 (Hz)	PIDF with wind	$-5.5x10^{-3}$	$1.7x10^{-3}$	13
	PIDF without wind	$-4.94x10^{-3}$	$1.89x10^{-3}$	19.5
	PIDF-PIDF with wind	$-2.89x10^{-3}$	$1.06x10^{-3}$	11.5
	PIDF-PIDF without wind	$-5.88x10^{-3}$	$1.1x10^{-3}$	11.5
	ANF-PIDF-PIDF with wind	$-3.13x10^{-3}$	$0.87x10^{-3}$	10.5
	ANF-PIDF-PIDF without wind	$-5.42x10^{-3}$	$1.47x10^{-3}$	11
ΔP_{tie12} (p.u)	PIDF with wind	$-2.18x10^{-4}$	$2.19x10^{-4}$	25
	PIDF without wind	$-5.66x10^{-4}$	$3.5x10^{-4}$	19
	PIDF-PIDF with wind	$-9.42x10^{-5}$	$3.13x10^{-5}$	25
	PIDF-PIDF without wind	$-1.02x10^{-4}$	$0.59x10^{-4}$	27.5
	ANF-PIDF-PIDF with wind	$-6.7x10^{-5}$	$4.01x10^{-5}$	18.5
	ANF-PIDF-PIDF without wind	$-6.8x10^{-5}$	$4.31x10^{-5}$	22
ΔP_{tie23} (p.u)	PIDF with wind	$-1.85x10^{-4}$	$2.42x10^{-4}$	19.5
	PIDF without wind	$-5.66x10^{-4}$	$3.5x10^{-4}$	29.5
	PIDF-PIDF with wind	$-6.5x10^{-6}$	$9.78x10^{-6}$	28.5
	PIDF-PIDF without wind	$-6.64x10^{-4}$	$1.1x10^{-4}$	20.5
	ANF- PIDF-PIDF with wind	$-1.21x10^{-4}$	$0.84x10^{-4}$	17.5

Preprints (www.preprints.org) | NOT PEER-REVIEWED | Posted: 22 November 2022 doi:10.20944/preprints202211.0422.v1

	ANF-PIDF-PIDF without wind	$-1.17x10^{-4}$	$0.96x10^{-4}$	18.5
ΔP_{tie13} (p.u)	PIDF with wind	$-1.4x10^{-4}$	$0.97x10^{-4}$	20.5
	PIDF without wind	$-7.4x10^{-5}$	$6.82x10^{-5}$	29
	PIDF-PIDF with wind	$-0.25x10^{-5}$	$3.82x10^{-5}$	23.5
	PIDF-PIDF without wind	$-5.66x10^{-5}$	$11.3x10^{-5}$	20.5
	ANF-PIDF-PIDF with wind	$-2.3x10^{-5}$	$0.92x10^{-5}$	16.5
	ANF-PIDF-PIDF without wind	$-4.74x10^{-5}$	$7.5x10^{-5}$	18

3.2. *Dynamic system response analysis considering the impact of non-linearity*

Wind energy sources were incorporated into each area using an AGC at normal incidence. The skill optimization technique was used to optimize the suggested controller adaptive NF-PIDF-PIDF settings. The non-linearity system constraint in GRC is considered and optimized using the same control parameters as in the existing models. The critical analysis of the dynamic response in Figure.14 (a)-(f) clearly demonstrates that the proposed ANF-PIDF-PIDF controller incorporating wind power plants (WPPs) considering generation rate constraint (GRC) gives improved dynamic performance in terms of peak deviation, oscillation, and settling time. Table 6 compares the suggested optimal adaptive NF-PIDF-PIDF controller with the traditional cascaded PIDF and simple PIDF controller with a wind power plant and displays the percentage improvement in undershoot and settling time. In comparison to the only PIDF controller, the percentage improvement in overshoot (OS) and settling time (T_s) of $\Delta f1$ with the optimal adaptive NF-PIDF-PIDF controller is 68.21% and 43.88%, respectively. Similarly, the suggested adaptive NF-PIDF-PIDF controller improves overshoot (OS) and settling time (T_s) of $\Delta f2$ by 65.75% and 23.57%, respectively, compared to the traditional PIDF controller. Similarly, $\Delta f3$ improves overshoot (OS) and settling time (T_s) by 57% and 22.83%, respectively, compared to the traditional PIDF controller. In addition, as compared to the simple PIDF, classical PIDF controller, and adaptive NF-PIDF-PIDF controller improves ΔP_{tie12}; ΔP_{tie23} and ΔP_{tie13} overshoot (OS) and settling time (T_s) by (80.89%, 40.78%), (83.46%, 40.58%) and (56.24%, 24%) respectively. As a result of the investigation, as mentioned earlier, the SOA-based adaptive NF-PIDF-PIDF controller claims to provide significant improvements.

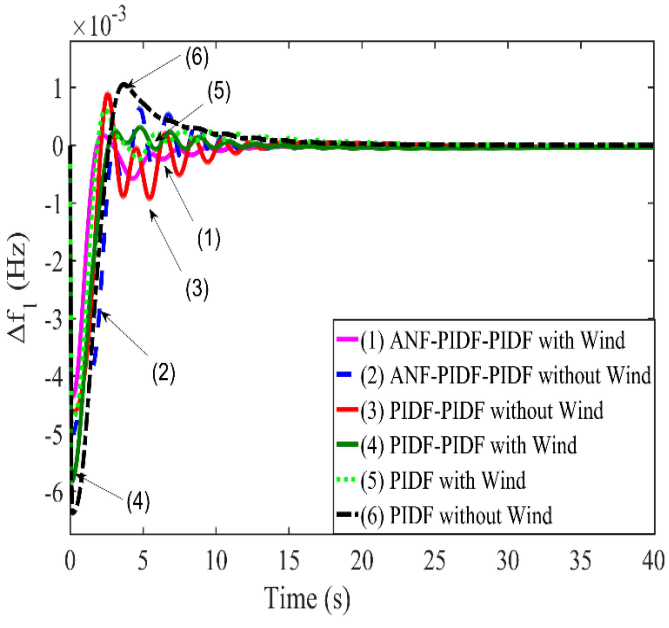

(**a**)

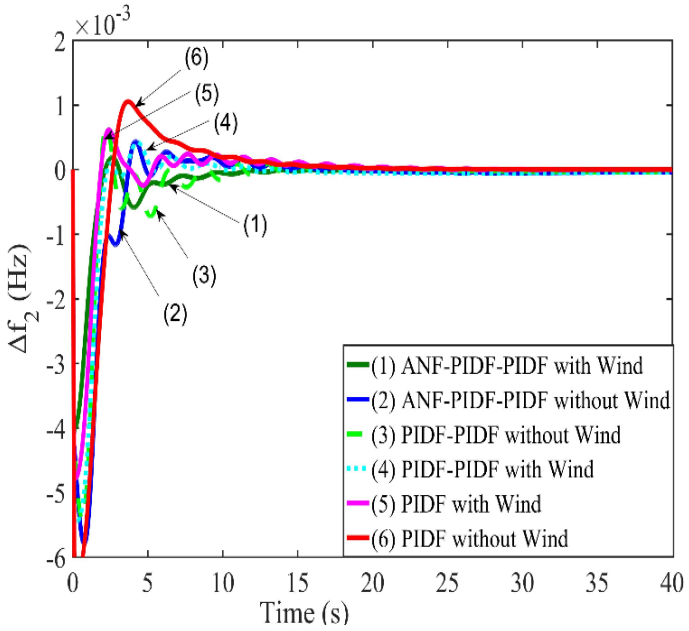

(**b**)

Preprints (www.preprints.org) | NOT PEER-REVIEWED | Posted: 22 November 2022 doi:10.20944/preprints202211.0422.v1

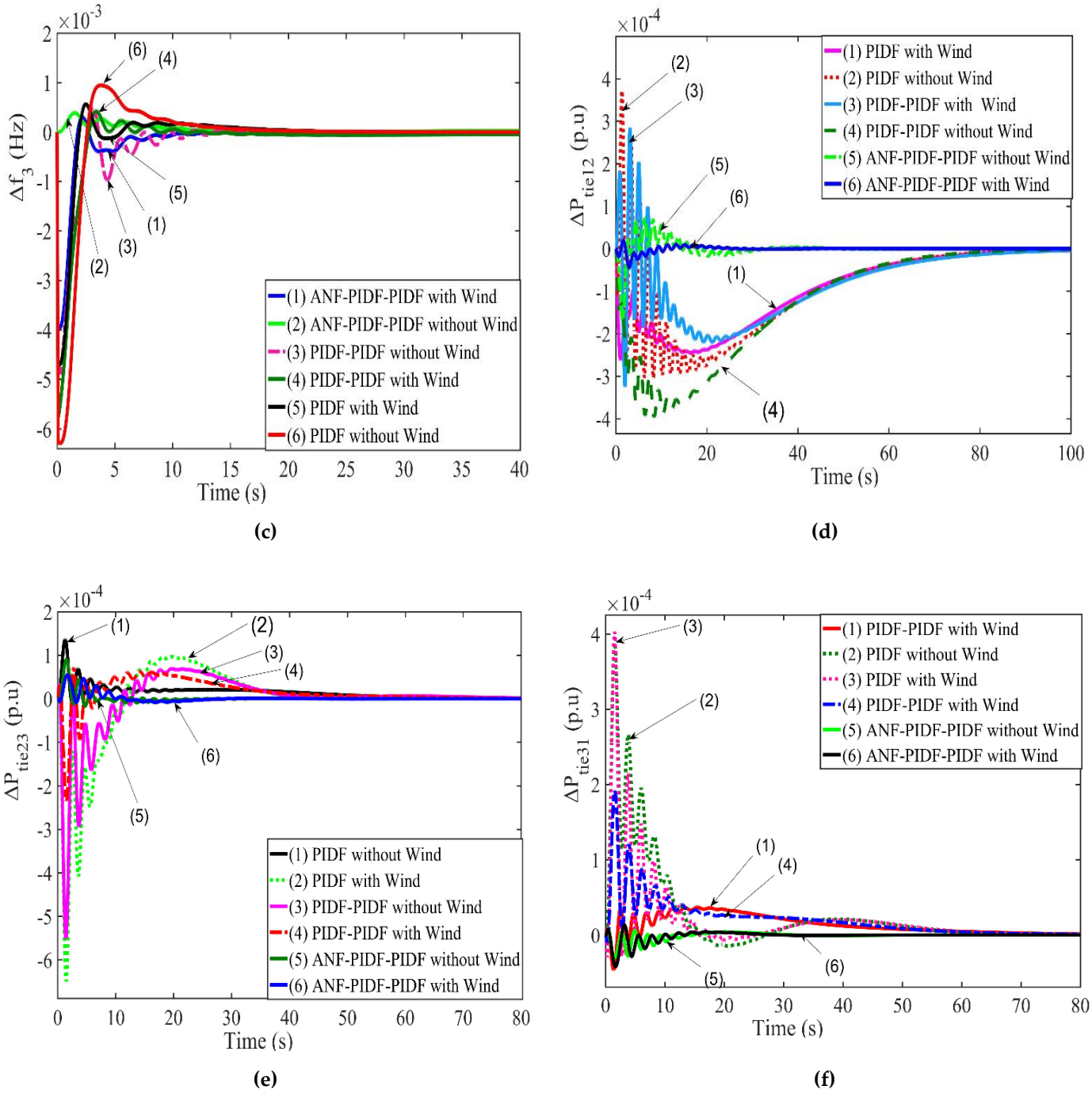

Figure.14. The dynamic responses comparison with various controllers with and without considering wind power plants (WPP)
(a) deviation in area-1 frequency , (b) deviation in area-2 frequency, (c) deviation in area-3 frequency (d) deviation in tie line power connecting area-1 and area-2, (e) deviation in tie line power connecting area-2 and area-3, (f) deviation in tie line power connecting area-1 and area-3

Preprints (www.preprints.org) | NOT PEER-REVIEWED | Posted: 22 November 2022 doi:10.20944/preprints202211.0422.v1

Table.6: Performance comparison PIDF, cascaded PIDF and ANF-PIDF-PIDF controller by considering non-linearity (GRC)

Control action	controllers	Undershoot	Overshoot	Settling time(s)
Δf_1 (Hz)	PIDF	$-4.68x10^{-3}$	$0.55x10^{-3}$	32
	PIDF-PIDF	$-5.11x10^{-3}$	$0.54x10^{-3}$	27
	ANF-PIDF-PIDF	$-4.28x10^{-3}$	$0.21x10^{-3}$	19
Δf_2 (Hz)	PIDF	$-4.6x10^{-3}$	$0.50x10^{-3}$	24.5
	PIDF-PIDF	$-5.6x10^{-3}$	$0.427x10^{-3}$	23
	ANF-PIDF-PIDF	$-4.01x10^{-3}$	$0.2x10^{-3}$	19
Δf_3 (Hz)	PIDF	$-4.62x10^{-3}$	$0.54x10^{-3}$	22
	PIDF-PIDF	$-4.48x10^{-3}$	$0.23x10^{-3}$	20.5
	ANF-PIDF-PIDF	$-3.97x10^{-3}$	$0.32x10^{-3}$	18
ΔP_{tie12} (p.u)	PIDF	$-1.6x10^{-4}$	$6.86x10^{-5}$	45
	PIDF-PIDF	$-3.04x10^{-4}$	$3.7x10^{-4}$	40
	ANF-PIDF-PIDF	$-2.6x10^{-4}$	$0.14x10^{-6}$	28
ΔP_{tie23} (p.u)	PIDF	$-1.73x10^{-5}$	$9.01x10^{-5}$	45
	PIDF-PIDF	$-6.5x10^{-5}$	$0.97x10^{-5}$	40
	ANF-PIDF-PIDF	$-8.3x10^{-6}$	$1.4x10^{-5}$	28
ΔP_{tie13} (p.u)	PIDF	$-2.99x10^{-5}$	$6.01x10^{-5}$	48
	PIDF-PIDF	$-1.5x10^{-5}$	$3.88x10^{-4}$	46
	ANF-PIDF-PIDF	$-4.65x10^{-5}$	$2.69x10^{-5}$	38

3.3. *Dynamics response performance considering parallel AC-HVDC tie-lines*

The results presented is for the case considering a hydrothermal integrated wind farm system that includes a parallel AC-HVDC tie-line, the adaptive Neuro-Fuzzy cascaded PIDF controller, and the SOA optimization algorithm. Figure. 15 (a-f) compares the parallel AC-HVDC tie-lines' dynamic response with the existing system for different frequency deviations through 6 cases. For improved power transfer among interconnected areas, AC tie-lines are being considered to be replaced by AC/HVDC tie-lines. The system considered the present controller, whose performance are depicted in Figure 15 (a)-(f). The response performance comparison reveals that the AC/HVDC tie-lines has less settling time, oscillation number, and peak deviations. Moreover the crucial finding from Figure 15 (a)–(f) is that the system frequency deviations and inter-area tie-power are fast driven back to zero when using the suggested method.

In Figure. 15(a), the dynamic response of AC tie-line and parallel AC-HVDC tie-lines are compared considering deviation in area 1 frequency. In Figure. 15(b), the dynamic response of AC tie-line and parallel AC-HVDC tie-lines are compared in area 2 frequency. In Figure. 15(c), the dynamic response of AC tie-line and parallel AC-HVDC tie-lines are compared in area 3 frequency. In Figure. 15(d), the dynamic response of AC tie-line and parallel AC-HVDC tie-lines are compared considering deviation in tie line power connecting area-1 and area-2. In Figure. 15(e), the dynamic response of AC tie-line and parallel AC-HVDC tie-lines are compared considering deviation in tie line power connecting area-2 and area-3. In Figure. 15(f), the dynamic response of AC tie-line and parallel AC-HVDC tie-lines are compared considering deviation in tie line power connecting area-1 and area-3. The response performance comparison reveals that the AC/HVDC tie-lines have less settling time, peak oscillation, and peak deviations.

Preprints (www.preprints.org) | NOT PEER-REVIEWED | Posted: 22 November 2022 doi:10.20944/preprints202211.0422.v1

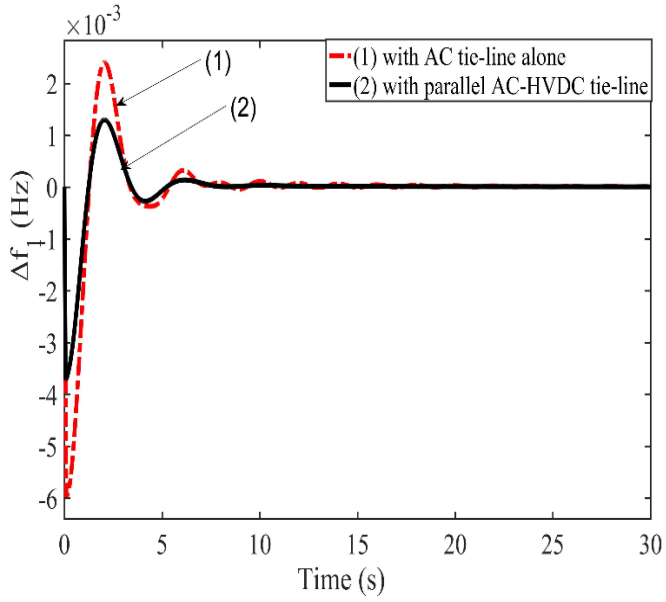

(a)

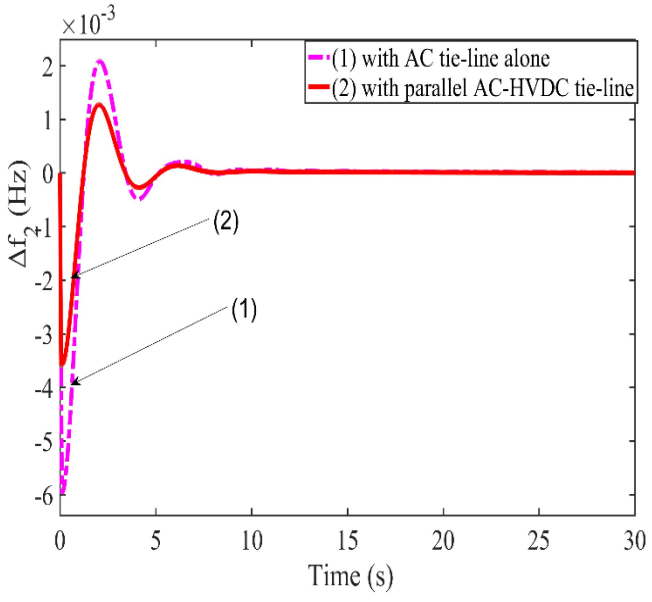

(b)

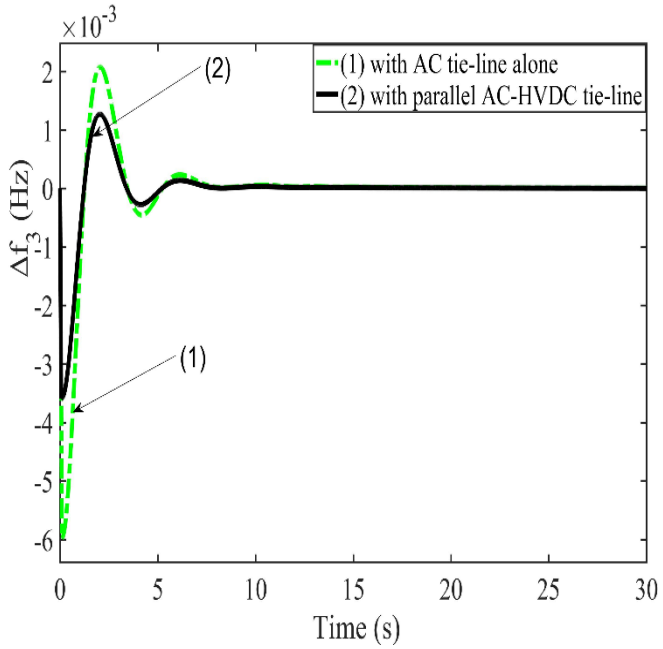

(c)

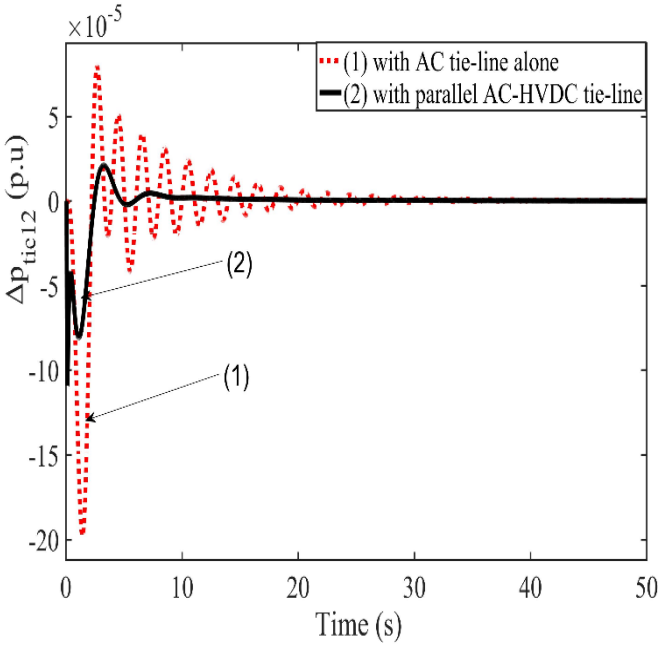

(d)

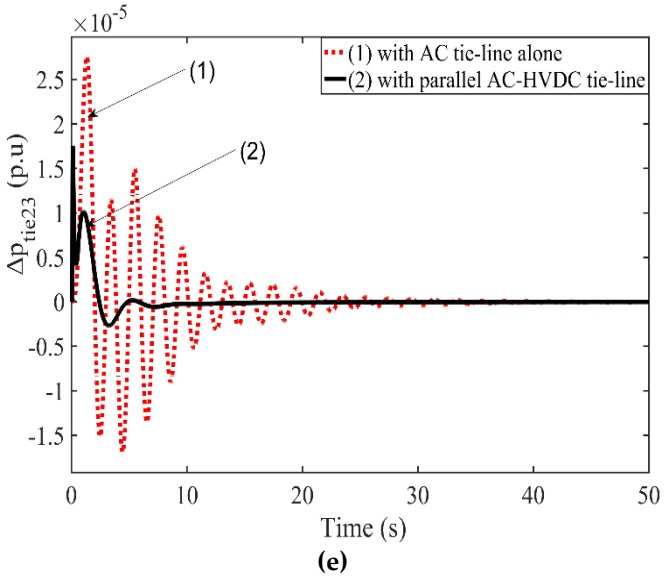

(e)

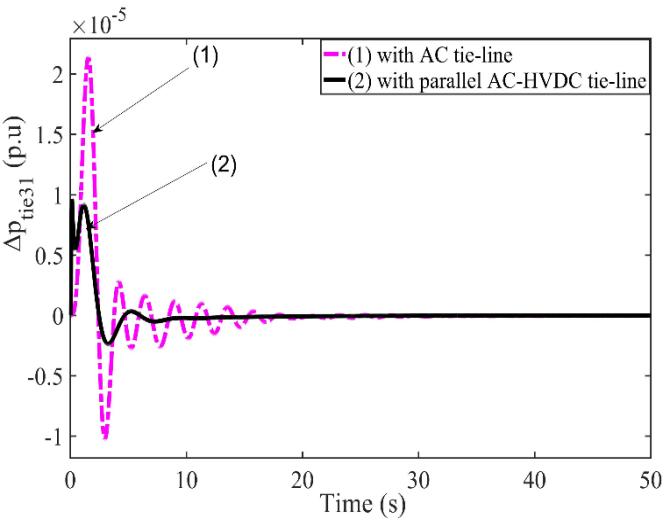

(f)

Preprints (www.preprints.org) | NOT PEER-REVIEWED | Posted: 22 November 2022 doi:10.20944/preprints202211.0422.v1

Figure.15. The dynamic responses comparison of AC tie-line with parallel AC-HVDC tie-line considering wind power plants (WPP). deviation in area-1 frequency , (b) deviation in area-2 frequency, (c) deviation in area-3 frequency (d) deviation in tie line power connecting area-1 and area-2, (e) deviation in tie line power connecting area-2 and area-3, (f) deviation in tie line power connecting area-1 and area-3

3.4. *Sensitivity analysis of the Proposed Controller*

The dynamic responses for various loading conditions with optimal value and system loading situations with optimal nominal conditions are shown in Figures.16 and 17. It has been proven that every dynamic response was optimal. A sensitivity analysis of a controller is employed to assess its resilience in different perturbing situations, like parameter changes, system loading variations, and system nonlinearities. The sensitivity analysis is examined in this section by adjusting the system loading with various magnitudes for each area, ±25% loading systems. The parameters K_{pss}, T_{pss}, B_s, D_s, and T_w, deviate from their nominal values as the system loading changes. Those values are given in Appendix-A. SOA schemes are used to optimize the controller parameters for this system. Table 7 shows the dynamic system responses and compares them to the corresponding 50% loading. Under both loading circumstances, the reactions are almost identical. It could be inferred that the presented adaptive Neuro-Fuzzy-cascaded PIDF controller's optimal values at nominal loading are reliable and that the controller's settings do not need to be reset for substantial variations in systems loading.

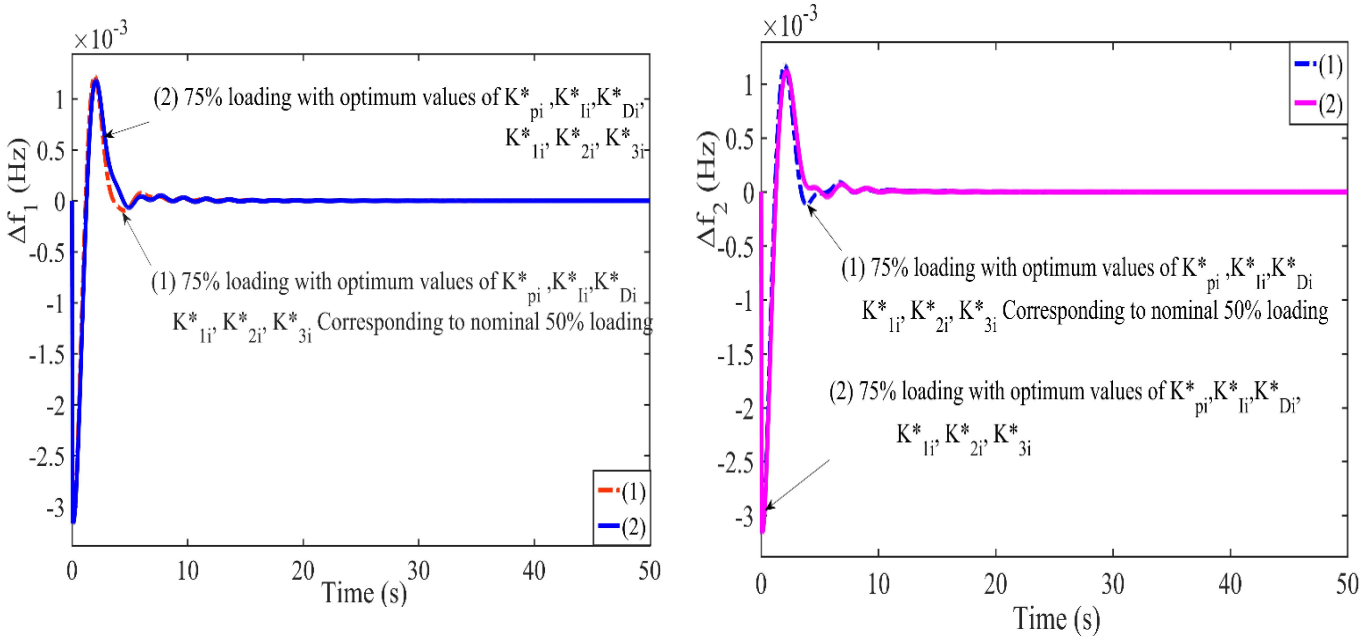

Preprints (www.preprints.org) | NOT PEER-REVIEWED | Posted: 22 November 2022 doi:10.20944/preprints202211.0422.v1

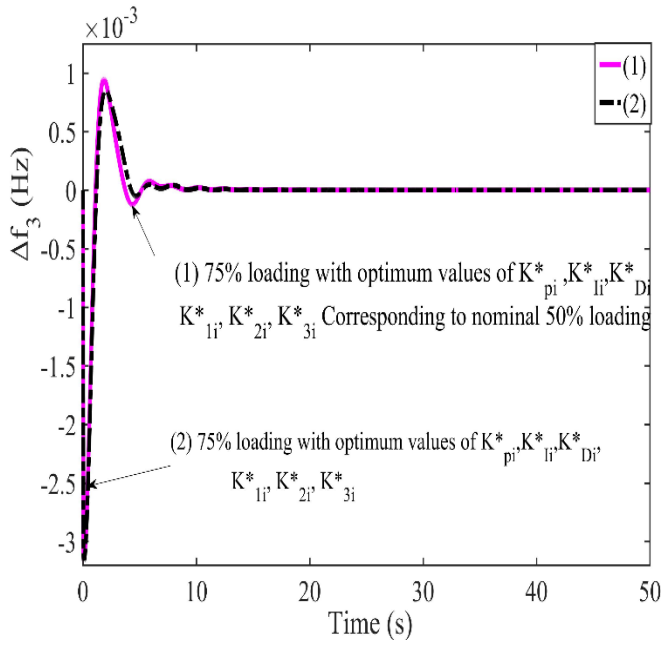

(c)

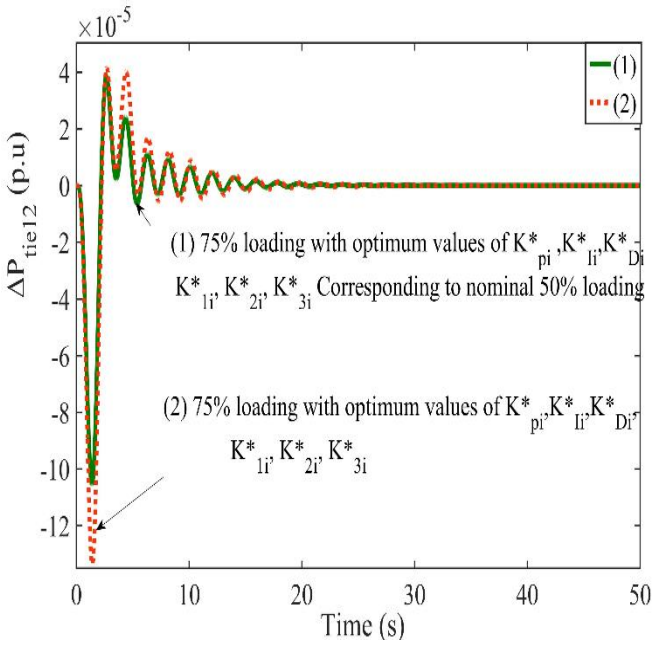

(d)

Figure.16. Comparison of dynamic responses for the proposed controller at 75% loading with optimum values corresponding to 75% loading and 50% loading. (a) Frequency deviation in area-1, (b) frequency deviation in area, (c) frequency deviation in area-3 (d) deviation in tie line power connecting area-1 and area-2 versus time

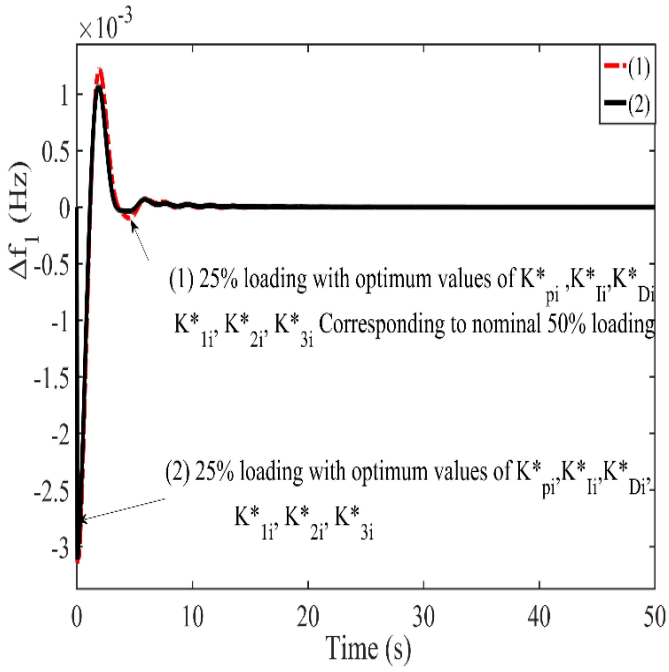

(a)

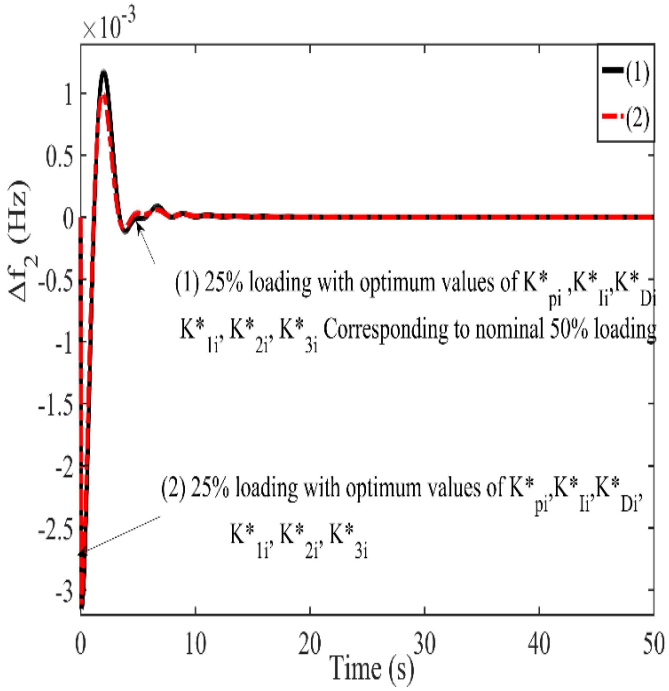

(b)

Preprints (www.preprints.org) | NOT PEER-REVIEWED | Posted: 22 November 2022 doi:10.20944/preprints202211.0422.v1

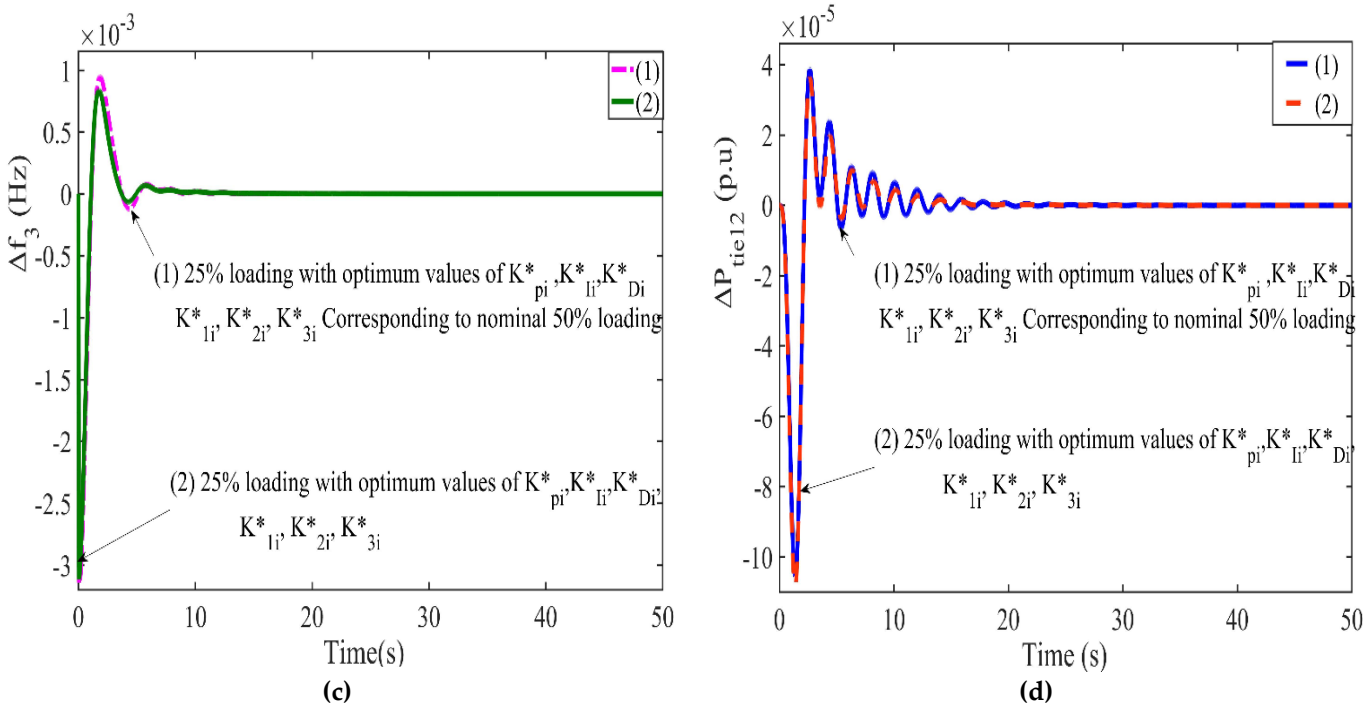

Figure.17. Comparison of dynamic responses for the proposed controller at 25% loading with optimum values corresponding to 25% loading and 50% loading. (a) Frequency deviation in area-1, (b) frequency deviation in area, (c) frequency deviation in area-3 (d) deviation in tie line power connecting area-1 and area-2 versus time

Table.7: The performance compares the Effect of changing the Gains and time Constant under different loading conditions.

Control action	Loading conditions	Undershoot	Overshoot	Settling time(s)
Δf_1 (Hz)	50%	$-3.154x10^{-3}$	$1.222x10^{-3}$	13.5
	75%	$-3.164x10^{-3}$	$1.183x10^{-3}$	15.5
	25%	$-3.115x10^{-3}$	$1.074x10^{-3}$	11.5
Δf_2 (Hz)	50%	$-3.154x10^{-3}$	$1.174x10^{-3}$	11
	75%	$-3.163x10^{-3}$	$1.126x10^{-3}$	11
	25%	$-3.115x10^{-3}$	$0.997x10^{-3}$	10.5
Δf_3 (Hz)	50%	$-3.153x10^{-3}$	$0.947x10^{-3}$	11
	75%	$-3.162x10^{-3}$	$0.85x10^{-3}$	11
	25%	$-3.115x10^{-3}$	$0.847x10^{-3}$	9.5
ΔP_{tie12} (p.u)	50%	$-1.049x10^{-4}$	$3.86x10^{-4}$	23
	75%	$-1.337x10^{-4}$	$0.421x10^{-5}$	27
	25%	$-1.088x10^{-4}$	$0.346x10^{-4}$	18
ΔP_{tie23} (p.u)	50%	$-5.93x10^{-5}$	$3.44x10^{-5}$	20.5
	75%	$-6.37x10^{-5}$	$3.58x10^{-5}$	22
	25%	$-4.97x10^{-5}$	$2.575x10^{-5}$	15.5
ΔP_{tie13} (p.u)	50%	$-2.94x10^{-5}$	$6.14x10^{-5}$	17
	75%	$-3.02x10^{-5}$	$6.95x10^{-5}$	18.5
	25%	$-2.28x10^{-5}$	$5.52x10^{-5}$	16.5

 doi:10.20944/preprints202211.0422.v1

Table 5 the performance compares the Effect of changing the Gains and time Constant under different loading condition. According to numerical evaluation the result shows the dynamic system responses compared to the corresponding 50% loading. Under both loading circumstances, the reactions are almost to be identical. Tables also show that 25% loading condition the settling time (t_s) was shorter than that of 75% loading.

4. Conclusion

In this research, a software novelty is presented through the maiden application of the skill optimization for the gains of the scaling factors of controller for AGC applications. The SOA is shown to be better in terms of convergence speed. The comparison of the SOA with other optimization algorithms for unimodal functions is presented to demonstrate this. Apart from this software novelty, a technical novelty is presented through the use of an adaptive Neuro-Fuzzy cascaded PIDF-AGC for improving the performances of a hybrid hydrothermal power system incorporated with wind energy sources. The present adaptive Neuro-Fuzzy cascaded PIDF controller's input-output scaling factors and gains are efficiently optimized using the novel Skill optimization Algorithm (SOA). Regarding efficiency, the current SOA- adaptive Neuro-Fuzzy cascaded PIDF controller is shown to be more efficient than the classic SOA-PIDF and cascaded PIDF controller. Furthermore, many scenarios are built to test the proposed controller's resilience and sensitivity to different loading situations, system parameter fluctuations, and nonlinearity. According to the simulation outcomes, the proposed SOA- adaptive Neuro-Fuzzy cascaded PIDF controller is more effective than traditional controllers. The simulation results demonstrate that the optimized adaptive Neuro-Fuzzy cascaded PIDF controller assures the least amount of damping oscillation with a better settling time compared to a simple PIDF controller response with and without addressing the effects of nonlinearity. Furthermore, the impact of the parallel AC-HVDC tie-line system on the dynamic system is compared to that of the conventional AC tie-line system, and better dynamic performances are obtained. The effectiveness of the proposed controller was evaluated using a sensitivity analysis by changing the system parameters by ± 25% loading. The load of the hydrothermal system is efficiently shared by integrating wind power plant units into hydrothermal units through parallel operation, which also considerably enhances the tie line power exchange from one area to another. As a result, in the case of a multi-area multi-source AGC power system, the skill optimization algorithm-based adaptive Neuro-Fuzzy cascaded PIDF controller may be utilized to manage hydrothermal power frequency and tie-line power efficiently. The optimized adaptive Neuro-Fuzzy cascaded PIDF-based AGC controller integrating wind energy sources reduces oscillation amplitude on average by 70%, significantly less than the solely conventional controllers.

Author Contributions:

Author Contributions: For research articles with several authors, a short paragraph specifying their individual contributions must be provided. The following statements should be used “Conceptualization, A.R. ,R.K. ,B.E. and J.R.; methodology, A.R.; software, A.R.; validation, A.R. ,R.K. ,B.E. and J.R.. and Z.Z.; formal analysis, A.R.; investigation, A.R.; resources, A.R.; data curation, A.R.; writing—original draft preparation, A.R.; writing—review and editing, A.R.; visualization, A.R.; supervision, R.K. ,B.E. and J.R.. ; project administration, A.R.; All authors have read and agreed to the published version of the manuscript.”

Funding: This research received no external funding

Data Availability Statement: The data will be made available after publication

Acknowledgments: We acknowledge Vellore Institute of Technology for providing laboratory facilities and softwars without which this research cannot be done.

 doi:10.20944/preprints202211.0422.v1

Conflicts of Interest: The authors declare no conflict of interest.

Appendix A

Table A1. Abbreviations and Nomenclature

Acronyms	Definition
AGC	Automatic Generation Control
PIDF	proportional-integral-derivative with filter
ANN	Artificial Neural Network
GRC	Generation Rate Constant
SOA	Skill Optimization Algorithm
ISE	integral square error
HVDC	high voltage direct current
ACE	area control error
AVR	automatic voltage regulator
ANF	Adaptive Neuro-fuzzy controller
STPP	Solar Thermal Power Plant
ALFC	automatic load frequency control
SLD	Step Load Disturbance
ITAE	Integral of the time weighted absolute error
ITSE	Integral time square error
IAE	Integral absolute error
WPPs	Wind Power Plants
RTP	Reheated Thermal Power
GTRT	Reheated Turbine
GGRT	Speed Governing method
HPP	Hydro power plant
SLP	Step Load Perturbations
FIS	Fuzzy Interfacing System
FLC	Fuzzy Logic Control

Nomenclature	Definition
f	nominal system frequency (Hz)
i	subscript referred to area i (1–3)/ superscript denotes optimum value
P_{ri}	rated power of area i (MW)
Hi	inertia constant of area i (s)
T12, T23, T13	synchronizing coefficients
Ri	governor speed regulation parameter of area i (Hz/p.u MW)
Tgi	steam governor time constant of area i (s)
K_{ri}	steam turbine reheat coefficient of area i
T_{ri}	steam turbine reheat time constant of area i (s)
T_{ti}	steam turbine time constant of area i (s)
Bi	frequency bias constant of area i
T_{pi}	2Hi/(f _ Di)
K_{pi}	1/Di (Hz/p.u)
Bi	area frequency response characteristics of area i (=Di + 1/Ri)
Tw	water starting time for hydro turbine (s)
Δfi	incremental change in frequency of area i (Hz)
ΔP_{gi}	incremental generation of area i (p.u)

 doi:10.20944/preprints202211.0422.v1

$\Delta P_{tie\ i\_j}$	incremental change in tie line power connecting between area i and area j (p.u)
Di	ΔPDi/Δfi (p.u/Hz)
K_P, K_I,K_D	The gains of proportional, integral, derivative respectively
N	Low pass filter coefficient
J	cost index
*	superscript denotes optimum value

Appendix B

System data at nominal condition:

P_{r1} = 2000MW, P_{r2} = 6000MW, P_{r3} = 12000MW, Assume Initial loading = 50%, f = 60Hz, B1 = B2 = R3 = 0.4250 p.u.MW/Hz, Ri = 2.40 Hz/per unit MW, Tg = 0.080 s, Ptie,max = 200 MW, Tr = 10s, Kr = 0.5 Hi = 5s, Tt = 0.3s, , Di = 8.33∗10-3 p.u. MW/Hz, a12= −1/3, a23= −1/2, a13= −1/6, T_{12} = T_{23} = T_{13}= 0.0866 p.u.MW/rad, TR = 5s, Kp1 = Kp2 = Kp3 = 120 Hz/p.u.MW, Tp1 = Tp2 = Tp3 = 20s. Wind power: 50*2MW, Kw1=1.4, Kw2=1.25, Kw3=0.080, Tw1=0.6sec, Tw2=0.040sec. Hydro plant: Electrical governor parameters, kdh = 0.270, kph = 1.0, kih = 2.40, Tw = 1.0s.

HVDC: KDC = 0.5, TDC=0.03s

Table B1. Variation of parameters with varying system loading

System Loading	K_{ps}inHz/ p.u.MW	T_{ps}, in sec.	D, in p.u. MW/Hz
50%	120.0	20.0	8.3310^{-3}
75%	80	13.33	0.0125
25%	240	40	0.004167

Author Contributions: Conceptualization, A.R. ,R.K. ,B.E. and J.R.; methodology, A.R.; software, A.R.; validation, A.R. ,R.K. ,B.E. and J.R.. and Z.Z.; formal analysis, A.R.; investigation, A.R.; resources, A.R.; data curation, A.R.; writing—original draft preparation, A.R.; writing—review and editing, A.R.; visualization, A.R.; supervision, R.K. ,B.E. and J.R.. ; project administration, A.R.; All authors have read and agreed to the published version of the manuscript."

Funding: This research received no external funding

Data Availability Statement: The data will be made available after publication

Acknowledgments: We acknowledge Vellore Institute of Technology for providing laboratory facilities and softwars without which this research cannot be done.

Conflicts of Interest: The authors declare no conflict of interest.

References

1. Ram Babu, N., Bhagat, S.K., Saikia, L.C. *et al.* A Comprehensive Review of Recent Strategies on Automatic Generation Control/Load Frequency Control in Power Systems. *Arch Computat Methods Eng* (2022). https://doi.org/10.1007/s11831-022-09810-y
2. K. Jagatheesan and B. Anand, "Automatic generation control of three area hydro-thermal power systems with electric and Mechanical governor," 2014 IEEE International Conference on Computational Intelligence and Computing Research, Dec. 2014
3. L. C. Saikia, J. Nanda, and S. Mishra, "Performance comparison of several classical controllers in AGC for multi-area Interconnected Thermal System," *International Journal of Electrical Power & Energy Systems*, vol. 33, no. 3, pp. 394–401, Mar. 2011.
4. W. Tasnin and L. C. Saikia, "Comparative performance of different energy storage devices in AGC of multi-source system including Geothermal Power Plant," Journal of Renewable and Sustainable Energy, vol. 10, no. 2, p. 024101, Mar. 2018.
5. H.Alhelou, M.-E. Hamedani-Golshan, R. Zamani, E. Heydarian-Forushani, and P. Siano, "Challenges and opportunities of load frequency control in conventional, modern and future Smart Power Systems: A comprehensive review," Energies, vol. 11, no. 10, p. 2497, Oct. 2018.
6. N. Hakimuddin, I. Nasiruddin, T. S. Bhatti, and Y. Arya, "Optimal Automatic Generation Control with hydro, thermal, gas, and wind power plants in 2-area interconnected power system," Electric Power Components and Systems, Vol. 48, no. 6-7, pp. 558–571, Apr. 2020.
7. G. M. Meseret and L. C. Saikia, "AGC in the multi-area thermal system with integration of distribution generation on the frequency of the system using the classical PID & Hybrid Neuro-Fuzzy Controllers," IETE Journal of Research, pp. 1–10, Jun. 2022.
8. G. M. Meseret and L. C. Saikia, "A comparative performance analysis evaluation of Automatic Generation Control (AGC) of multi-area power system with the impact of HVDC links on the system frequency using the conventional PID and adaptive Neuro-fuzzy controller," IFAC-Papers Online, vol. 55, no. 1, pp. 138–143, May 2022.
9. B. Dekaraja and L. C. Saikia, "Impact of energy storage and flexible alternating current transmission devices in combined voltage and frequency regulation of multi-area Multisource Interconnected Power System," Energy Storage, Vol. 4, no. 3, pp. 1-17, Jan. 2022.
10. C. R. Balamurugan, "Three area power system load frequency control using Fuzzy Logic Controller," International Journal of Applied Power Engineering (IJAPE), Vol. 7, no. 1, pp. 18–26, Jan. 2018.
11. X. Wang, Y. Wang, and Y. Liu, "Dynamic load frequency control for high-penetration wind power considering wind turbine fatigue load," International Journal of Electrical Power & Energy Systems, vol. 117, p. 105696, May 2020.
12. Vigya, T. Mahto, H. Malik, V. Mukherjee, M. A. Alotaibi, and A. Almutairi, "Renewable generation-based hybrid power system control using fractional order-fuzzy controller," Energy Reports, vol. 7, pp. 641–653, Nov. 2021.
13. W. Tasnin and L. C. Saikia, "Comparative performance of different energy storage devices in AGC of multi-source system including Geothermal Power Plant," Journal of Renewable and Sustainable Energy, vol. 10, no. 2, p. 024101, Mar. 2018.
14. S. K. Ramoji and L. C. Saikia, "Utilization of electric vehicles in combined voltage-frequency control of multi-area thermal-combined cycle gas turbine system using two degree of freedom tilt-integral-derivative controller," Energy Storage, vol. 3, no. 4, Mar. 2021.
15. N. Hasan, I. Alsaidan, M. Sajid, S. Khatoon, and S. Farooq, "Hybrid MPC-based automatic generation control for dominant wind energy penetrated multisource power system," Modeling and Simulation in Engineering, vol. 2022, pp. 1–10, Jan. 2022.
16. M. Elsisi, M. Aboelela, M. Soliman, and W. Mansour, "Design of optimal model predictive controller for LFC of Nonlinear Multi-area Power System with energy storage devices," Electric Power Components and Systems, vol. 46, no. 11-12, pp. 1300–1311, Jul. 2018.
17. A. Abazari, H. Monsef, and B. Wu, "Load frequency control by developing wind farm using the Optimal fuzzy based PID Droop Controller," *IET Renewable Power Generation*, vol. 13, no. 1, pp. 180–190, Nov. 2018.
18. R. K. Sahu, S. Panda, and U. K. Rout, "De optimized parallel 2-DOF PID controller for load frequency control of power system with governor dead-band nonlinearity," *International Journal of Electrical Power & Energy Systems*, vol. 49, pp. 19–33, Jul. 2013.
19. T. Prakash and V. P. Singh, "A novel membrane computing inspired Jaya algorithm based automatic generation control of Multi-area Interconnected Power System," *Series in Machine Perception and Artificial Intelligence*, pp. 89–110, Sep. 2018.
20. N. C. Patel, K. Mohanty, B. Giri, and S. K. Ekka, "Load frequency control in two areas interconnected hydro-thermal power system utilizing ALO based FPI controller," *2022 International Conference on Intelligent Controller and Computing for Smart Power (ICICCSP)*, Jul. 2022.
21. M. N. Anwar and S. Pan, "A new PID load frequency controller design method in frequency domain through direct synthesis approach," Int. J. Electric. Power Energ. Syst., vol. 67, pp. 560-569, May 2015.
22. Y. Sharma and L. C. Saukia, "Automatic generation control of a multi area ST-Thermal power system using grey wolf optimizer algorithm based classical controllers," Int. J. Electric. Power Energ. Syst., vol. 73, pp. 853-862, Dec. 2015.
23. M. H. Khooban and T. Niknam, "A new intelligent online fuzzy tuning approach for multi-area load frequency control: Self Adaptive Modified Bat Algorithm," Int. J. Electric. Power Energ. Syst., vol. 71, pp. 254–261, Oct. 2015.

24. A. Y. Abdelaziz and E. S. Ali, "Cuckoo search algorithm based load frequency controller design for nonlinear interconnected power system," Int. J. Electric. Power Energ. Syst., vol. 73, pp. 632-643, Dec. 2015.
25. B. K. Sahu, S. Pati, P. K. Mohanty, and S. Panda, "Teaching-learning based optimization algorithm based fuzzy-PID controller for automatic generation control of multi-area power system," Appl. Soft Comput., vol. 27, pp. 240—249, Feb. 2015.
26. R. K. Sahu, S. Panda, and G. T. C. Sekhar, "A novel hybrid PSO-PS optimized fuzzy PI controller for AGC in multi area interconnected power systems," Int. J. Electric. Power Energ. Syst., vol. 64, pp. 880–893, Jan. 2015.
27. J. Nanda, M. Sreedhar, and A. Dasgupta, "A new technique in hydro thermal interconnected automatic generation control system by using minority charge carrier inspired algorithm," Int. J. Electric. Power Energy Systems, vol. 68, pp. 259–268, Jun. 2015.
28. M. Shivaie, M. G. Kazemi, and M. T. Ameli, "A modified harmony search algorithm for solving load-frequency control of non-linear interconnected hydrothermal power systems," Sustain. Energ. Technol. Assess., vol. 10, pp. 53–62, Jun. 2015
29. L. H. Hassan, M. Moghavvemi, H. A. F. Almurib, K. M. Muttaqi, and V. G. Ganapathy, "Optimization of power system stabilizers using participation factor and genetic algorithm," Int. J. Electr. Power Energy Syst., vol. 55, pp. 668–679, Feb. 2014.
30. Y. A. Katsigiannis, P. S. Georgilakis, and E. S. Karapidakis, "Hybrid Simulated Annealing–Tabu Search Method for Optimal Sizing of Autonomous Power Systems With Renewables," IEEE Trans. Sustain. Energy, vol. 3, no. 3, pp. 330–338, Jul. 2012.
31. K. R. M. Vijaya Chandrakala and S. Balamurugan, "Simulated annealing based optimal frequency and terminal voltage control of multi source multi area system," Int. J. Electr. Power Energy Syst., vol. 78, pp. 823–829, Jun. 2016.
32. P. Acharjee, "Optimal power flow with UPFC using security constrained self-adaptive differential evolutionary algorithm for restructured power system," Int. J. Electr. Power Energy Syst., vol. 76, pp. 69–81, Mar. 2016.
33. Jong-Bae Park, Yun-Won Jeong, Joong-Rin Shin, and K. Y. Lee, "An Improved Particle Swarm Optimization for Nonconvex Economic Dispatch Problems," IEEE Trans. Power Syst., vol. 25, no. 1, pp. 156–166, Feb. 2010.
34. S. A. Taher and S. A. Afsari, "Optimal location and sizing of DSTATCOM in distribution systems by immune algorithm," Int. J. Electr. Power Energy Syst., vol. 60, pp. 34–44, Sep. 2014.
35. Pan and S. Das, "Fractional order fuzzy control of hybrid power system with renewable generation using chaotic PSO," ISA Transactions, vol. 62, pp. 19–29, May 2016.
36. A. Abou El-Ela, R. A. El-Sehiemy, A. M. Shaheen, and A. E.-G. Diab, "Design of cascaded controller based on Coyote optimizer for load frequency control in multi-area power systems with renewable sources," *Control Engineering Practice*, vol. 121, p. 105058, Apr. 2022.
37. M. A. El-Sayed, "Integrating Wind Energy into Weak Power Grid Using Fuzzy Controlled TSC Compensator," in International Conference on Renewable Energies and Power Quality (ICREPQ, 2010), Granada, Spain, 2010.
38. Fosha and O. Elgerd, "The megawatt-frequency control problem: A new approach via Optimal Control Theory," IEEE Transactions on Power Apparatus and Systems, Vol. PAS-89, no. 4, pp. 563–577, Apr. 1970.
39. Jagatheesan and B. Anand, "Automatic generation control of three area hydro-thermal power systems with electric and Mechanical governor," 2014 IEEE International Conference on Computational Intelligence and Computing Research, Dec. 2014, pp. 187-194.
40. Daraz, S. A. Malik, I. U. Haq, K. B. Khan, G. F. Laghari, and F. Zafar, "Modified PID controller for automatic generation control of multi-source interconnected power system using fitness dependent optimizer algorithm," PLOS ONE, vol. 15, no. 11, Nov. 2020.
41. Yousef, H.A.; Al-Kharusi, K.; Albadi, M.H.; Hosseinzadeh, N. Load Frequency Control of a Multi-Area Power System: An Adaptive Fuzzy Logic Approach. IEEE Trans. Power Syst. **2014**, 29, 1822–1830.
42. C. Das, A. K. Roy, and N. Sinha, "GA based Frequency Controller for solar thermal–diesel–wind hybrid energy generation/energy storage system," International Journal of Electrical Power & Energy Systems, vol. 43, no. 1, pp. 262–279, Dec. 2012.
43. D. Shakibjoo, M. Moradzadeh, S. U. Din, A. Mohammadzadeh, A. H. Mosavi, and L. Vandevelde, "Optimized type-2 fuzzy frequency control for Multi-Area Power Systems," IEEE Access, vol. 10, pp. 6989–7002, 2022.
44. Z. Zhang, E. Du, F. Teng, N. Zhang, and C. Kang, "Modeling Frequency Dynamics in unit commitment with a high share of renewable energy," IEEE Transactions on Power Systems, vol. 35, no. 6, pp. 4383–4395, Nov. 2020.
45. Pilla, Azar, and Gorripotu, "Impact of flexible AC transmission system devices on automatic generation control with a metaheuristic based Fuzzy PID Controller," Energies, vol. 12, no. 21, p. 4193, Nov. 2019.
46. S. K. Ramoji and L. C. Saikia, "Comparative performance of multiple energy storage systems in unified voltage and frequency regulation of power system including Electric Vehicles," Energy Storage, Jun. 2022.
47. N. K. Jena, S. Sahoo, B. K. Sahu, and K. B. Mohanty, "Design of fractional order Cascaded Controller for AGC of a Deregulated Power System," *Journal of Control, Automation and Electrical Systems*, vol. 33, no. 5, pp. 1389–1417, Feb. 2022.
48. Shayeghi, H.; Shayanfar, H.; Malik, O. Robust decentralized neural networks based LFC in a deregulated power system. Electric Power Syst. Res. **2007**, 77, 241–251.
49. Chaturvedi, D.K.; Satsangi, P.S.; Kalra, P.K. Load frequency control: A generalized neural network approach. Int. J. Elecrtr. Rical Power Energy Syst. **1999**, 21, 405–415.
50. S. Zhang, Y. Mishra, and M. Shahidehpour, "Fuzzy-logic based frequency controller for wind farms augmented with energy storage systems," IEEE Transactions on Power Systems, vol. 31, no. 2, pp. 1595–1603, Mar. 2016.

51. M. Sharma, S. Dhundhara, Y. Arya, and S. Prakash, "Frequency excursion mitigation strategy using a novel COA optimized fuzzy controller in Wind Integrated Power Systems," IET Renewable Power Generation, vol. 14, no. 19, pp. 4071–4085, Dec. 2020.
52. H. Givi and M. Hubalovska, "Skill Optimization Algorithm: A new human-based metaheuristic technique," Computers, Materials & Continua, vol. 74, no. 1, pp. 179–202, May 2022. https://doi.org/10.32604/cmc.2023.030379
53. M. I. Ali, A. A. Diab, A. A. Hassan, M. A. Mossa, and K. A. Denis, "Comprehensive comparison of the application of dynamic optimization algorithms for LFC of a double area system with the penetration of Renewable Energy Sources," 2022 4th International Youth Conference on Radio Electronics, Electrical and Power Engineering (REEPE), Mar. 2022.
54. R. Choudhary, J. N. Rai, and Y. Arya, "Cascade FPI-FOPTID controller with energy storage devices for AGC performance advancement of Electric Power Systems," Sustainable Energy Technologies and Assessments, vol. 53, p. 102671, Oct. 2022.
55. P. W. Nugroho, H. Du, W. Li, and G. Alici, "Implementation of Adaptive Neuro Fuzzy Inference System controller on magneto rheological damper suspension," in 2013 IEEE/ASME International Conference on Advanced Intelligent Mechatronics: Mechatronics for Human Wellbeing, AIM 2013, 2013, pp. 1399–1403.
56. H. Givi and M. Hubalovska, "Skill Optimization Algorithm: A new human-based metaheuristic technique," Computers, Materials & Continua, vol. 74, no. 1, pp. 179–202, May 2022.
57. B. Khokhar, S. Dahiya, and K. P. Parmar, "A novel fractional order proportional integral derivative plus second-order derivative controller for Load Frequency Control," International Journal of Sustainable Energy, vol. 40, no. 3, pp. 235–252, Aug. 2020.
58. Lal, D.K.; Barisal, A.K.; Tripathy, M. Grey Wolf Optimizer Algorithm Based Fuzzy PID Controller for AGC of Multi-area Power System with TCPS. Procedia Comput. Sci. **2016**, 92, 99–105.
59. Behera, T. K. Panigrahi, P. K. Ray, and A. K. Sahoo, "A novel cascaded PID controller for Automatic Generation Control Analysis with renewable sources," IEEE/CAA Journal of Automatica Sinica, vol. 6, no. 6, pp. 1438–1451, Nov. 2019.
60. P. S. Georgilakis, "Technical Challenges Associated with the Integration of Wind Power into Power Systems," Renewable and Sustainable Energy Reviews, vol. 12, pp. 852-863, 2008.